



HAL
open science

Structure Dominated Two-Dimensional Turbulence : Formation, Dynamics and Interactions of Dipole Vortices

Ö Gürcan

► **To cite this version:**

Ö Gürcan. Structure Dominated Two-Dimensional Turbulence : Formation, Dynamics and Interactions of Dipole Vortices. *Journal of Physics A: Mathematical and Theoretical*, 2023, 56 (28), pp.285701. 10.1088/1751-8121/acdc6b . hal-04212192

HAL Id: hal-04212192

<https://hal.science/hal-04212192>

Submitted on 20 Sep 2023

HAL is a multi-disciplinary open access archive for the deposit and dissemination of scientific research documents, whether they are published or not. The documents may come from teaching and research institutions in France or abroad, or from public or private research centers.

L'archive ouverte pluridisciplinaire **HAL**, est destinée au dépôt et à la diffusion de documents scientifiques de niveau recherche, publiés ou non, émanant des établissements d'enseignement et de recherche français ou étrangers, des laboratoires publics ou privés.

Structure Dominated Two-Dimensional Turbulence : Formation, Dynamics and Interactions of Dipole Vortices

Ö. D. Gürçan

Laboratoire de Physique des Plasmas, CNRS, Ecole Polytechnique, Sorbonne
Université, Université Paris-Saclay, Observatoire de Paris, F-91120 Palaiseau, France

Abstract. Two dimensional turbulence in geophysical fluids and plasma physics tends to be spotty, intermittent and rich in large scale structures such as coherent vortices or zonal flows, due to various mechanisms of self organization. Nonlinear solutions that rely on the vanishing of nonlinearity, especially the dipole vortex solution, stand out as key aspects of this structure dominated turbulence state. Using numerical simulations, it is demonstrated that an initial condition with a small number of high intensity turbulent patches, evolves towards a state dominated by coherent structures, and in particular dipole vortices, as each patch is organized into a finite number of dipole vortices that are ejected from this initially active region. In order to study the details of this process, an initial condition of two Gaussian peaks of the stream function is considered, and it was shown to result in a Chaplygin-Lamb dipole if the peaks have the same amplitude, or a Flierl-Stern-Whitehead dipole that rotates in the direction implied by the excess of vorticity if they do not. Analytical estimates for the velocity, the radius and the radius of curvature of the resulting dipole vortex is given in terms of the peaks and widths of the initial conditions. These are then verified by a detailed comparison of the analytical form of the vorticity of the dipole vortex and its numerical realization. It is argued that since these coherent structures are spared from the strong shear forces normally exerted by the nonlinearities, and can coexist with other localized solutions, or large scale flow patterns, they provide the backbone of the structure dominated or “sporadic” turbulent state in two dimensions, on top of which other structures, waves and instabilities can develop. In order to elucidate these, a number of collision scenarios are considered. It is also shown that a simple two point vortex approximation to a dipole vortex seems to be appropriate for describing their evolution far from each-other, or for computing head on collisions between two or more dipole vortices, but not in the case of close or grazing collisions or their interaction with a nontrivial large scale flow.

1. Introduction

Turbulence, which manifests itself as a duality of chaotic dynamics and self-organization of a fluid-like system across a large range of scales, is ubiquitous in nature[1]. Its study is vital for many problems in science from biology to geophysics, from plasmas to lasers, and from the smallest scales that we can observe to the largest. When studied in the strict confines of two dimensions, it has peculiar features, different from its three dimensional cousin. It is commonly observed in numerical simulations, for example, that while three dimensional turbulence is intermittent -in the sense of the deviation of the scaling of the power law exponent [i.e. ζ_n in $S_n(\ell) \propto \ell^{\zeta_n}$] of the n th order structure function [defined as $S_n(\ell) \equiv |v(x+\ell) - v(x)|^n$] as a function of its order n , from the Kolmogorov scaling- [2, 3, 4], two dimensional turbulence is mostly non-intermittent, especially for the inverse cascade range[5, 6] -even though the full story is a bit more complicated as usual-. Intermittence, defined this way is a statistical feature of the scaling properties of homogeneous, isotropic, fully developed turbulence state and not a universal feature (i.e. at least, not always) of the equations or their dimensionality. As a matter of fact quasi-two dimensional turbulence in the atmosphere and the ocean as well as in laboratory and space plasmas are often spotty or “intermittent” but only in the sense that it does not satisfy the common assumptions of isotropy and homogeneity. In particular the presence of organized large scale flow patterns, such as zonal flows[7, 8], which are manifestations of some kind of anisotropic “inverse cascade” are common features of this kind of turbulent state, with peculiar dynamical behavior such as predator-prey evolution[9, 10] also implying temporal intermittency, again common in these systems.

The principal goal of this paper is to establish, the extremely intermittent turbulent state as a particular regime called *structure dominated turbulence*, or sporadic turbulence following Mandelbrot[11] -that is if we define a parameter d which determines the degree of spottiness of turbulence where $d = 1$ representing homogeneous turbulence and $d = 0$ being a single peak, for $d \ll 1$ or more exactly for $d \lesssim 1$, we get sporadic turbulence- not necessarily because of a statistical tendency of the homogeneous isotropic turbulence to intermittency, but because of external or initial conditions, or because the system is in the process of transition, or some other reason, such as the existence of additional physics that causes the system to favor formation of large or meso-scale coherent structures. This would suggest that we should use different tools based on spatial structures, their dynamics and interactions in order to study this particular state of turbulence instead of using statistical analysis that rely on concepts of turbulent cascade that are better adapted to the study of the homogeneous, isotropic turbulence states.

It is sometimes argued that the late phase of relaxation in two dimensional turbulence may give rise to a similar state of turbulence dominated by isolated coherent vortices[12, 13], even though the universality of this relaxation, especially in light of a discussion on the effects of external and initial conditions remain unclear. Nonetheless, it is well established that the general case of decaying two dimensional turbulence, can be

represented as a collection of interacting vortices, and described as an evolving network of vortical interactions[14].

Another distinctive, but not unrelated aspect of two dimensional turbulence, that is of essential importance to its dynamics, is the dual cascade of energy and enstrophy[15, 16], where the energy inverse cascades towards larger scales while the enstrophy cascades to smaller scales and gets dissipated. This exceptional feature of two dimensional turbulence gives rise to a mechanism of selective decay and therefore to formation of large scale structures that can be characterized as minimum enstrophy states, since the enstrophy that cascades to small scales get dissipated, while the energy that cascades to large scales lingers[17, 18, 19]. While it is sometimes argued that this happens via vortex mergers, resulting eventually in a single large scale dipole that is at the same time a minimum enstrophy state[20], it can also be inferred from self-adaptation through viscous selection[21] that in the context of spotty, sporadic turbulence would conceivably result in a number of coherent structures in the turbulent state, each of which are either locally minimum enstrophy states or specific dipole vortex solutions, meandering about due to their internal velocities, while being advected by the overall flow structure.

A variation of the idea of “selective decay“ can also be invoked in the more general, rather abstract sense that any structure that somehow survives in the turbulent state, must have a small nonlinear stress acting on it. This can be attributed to concepts in evolutionary statistics such as the Darwinian concept of the survival of the fittest: If the turbulent evolution proposes two candidate structures, one which feels a great amount of nonlinear stress and another that feels none, or little of it, the nonlinear forces will rapidly shear apart the former as it is not well adapted to them, while the latter will continue to survive[8]. In this sense the background turbulence plays the role of “environment” and the turbulent stresses due to nonlinearities provide the evolutionary pressure on structures. This process would eventually result in a state of depression, or suppression of nonlinearity [22, 23] where most of the quasi-steady state structures that are observed would have no nonlinear stress acting on them. Thus, sporadic two dimensional turbulence is this state dominated by coherent vortices and similar large scale patterns and structures as a result of selective decay and the concept of depletion of nonlinearity[24, 25]. There are analogues of this phenomenon in various other systems, such as for example the concept of dynamical alignment in MHD turbulence[26].

Since in a general sense, vortices are localized perturbations, and that a monopole structure lacks the means of self-propulsion, vortex pairs whose dynamics are studied in some detail [27], and in particular the dipole vortex configuration constitute the simplest self-propelling localized perturbation, and as such, is central to the study of structure dominated two dimensional turbulence. Similar to solitons[28], and their inverse scattering in various nonlinear systems such as the nonlinear Schrödinger equation[29], certain classes of initial conditions give rise to a finite number of dipole vortices that move at speeds defined by their amplitudes, involve in collisions respecting certain conserved quantities etc. Thus it can be argued that dipole vortices play the

role of *elementary particles* in sporadic two dimensional turbulence. They are also the dominant structures in thin films [30], oceans [31] and in superfluids such as Bose-Einstein condensates[32, 33]. The most notable example of these structures is the Chaplygin-Lamb (CL) dipole vortex[34], which is a class of circular vortex solutions of the two dimensional Euler equations with two regions of constant vorticity connected through a separatrix. In particular the case of the rotating dipole vortex, consisting of an asymmetric dipole vortex, which follows a phase locked circular orbit around its center of rotation [35] is of great interest as it generalizes the basic CL dipole vortex solution into the more general class of curved trajectories. We call those the FSW vortices (for Flierl, Stern and Whitehead) in order to distinguish them from the general class studied by Chaplygin (which apparently also includes the FSW case [34]) or the particular solution discussed by Lamb. Note that these solutions are possible to realize approximately, with relatively small error, in numerical simulations of two-dimensional Navier-Stokes equations with small viscosity.

In this paper, we show that a 2D Navier-Stokes system initialized with a small number of high intensity turbulent patches, evolves towards a state of sporadic turbulence, dominated by dipole vortices, through a mechanism, argued to be related to rapid selective decay by which each puff is decomposed into a number of dipole vortices, moving in opposite directions in order to conserve momentum and circulation. In order to study the mechanism in more detail, we further consider an initial condition with two nearby peaks of opposite signs of the stream function, and observe that it forms a dipole vortex that moves together in the direction of the flow between the two vortices. Depending on which peak has the larger peak vorticity one gets a rotating dipole vortex that rotates in the direction imposed by that peak. We show that this process is robust and results in an actual FSW vortex solution to the extent that it is numerically realizable, as confirmed by a detailed comparison of its radial and poloidal structure to the analytical form expected from the FSW dipole vortex. In fact, the final parameters of the dipole vortices such as their velocity, amplitude, radius and the radius of curvature of its orbit, can all be estimated from the initial parameters of the two Gaussian peaks using energy and enstrophy conservation, in addition to conservation of circulation inside the initial separatrices. It can be shown for example that the velocity of the dipole can be estimated in the inviscid case, and the effect of viscosity can be incorporated into this estimation as a slow decay due to an effective friction with the rate of decay given by νk_a^2 , where $k_a = 2\pi/\lambda_a$ and $\lambda_a = 2aj_{01}/j_{11}$ is the distance between the peaks of vorticity in a dipole vortex, where $j_{i\ell}$ are the ℓ th zero of the Bessel function $J_i(x)$. Furthermore, since a Gaussian peak for the stream function, when viewed as a vorticity distribution (i.e. Laplacian of a Gaussian), has a peak vorticity of one sign and an outer rim vorticity of the opposite sign, the resulting primary dipole also has a weaker sibling that consists of the rim vorticities, moving (and rotating) in the opposite direction.

We also discuss how and when a dipole vortex can coexist with a different (for example periodic) nonlinear solution and how it interacts with a large scale sheared flow.

This is done by discussing a class of exact, periodic solutions of the Euler equations such as the Stuart vortex [36], that can be used to represent a somewhat realistic large scale background flow, and considering the interactions between these solutions and localized dipole vortices numerically. Collisions between dipole vortices in circular orbits are also considered. In particular it was observed that when two FSW vortices of equal and opposite net vorticities collide in a head-on collision, they form two CL dipole vortices that move in the opposite directions in the direction normal to the circular orbits of the initial vortices. Similarly head on collisions between two FSW vortices of unequal net vorticities, result in two new FSW vortices that have different orbital radii and different sizes. We find that the use of a simple two point vortex approximation[37, 38, 39] seems to be appropriate for computing head on collisions between dipole vortices, but not in the case of close or grazing collisions or their interaction with a nontrivial large scale flow.

We also discuss briefly a tripolar configuration, consisting of a larger vortex of one sign of vorticity between two smaller vortices of the opposite sign. If the three vortices are arranged symmetrically, and close together, the resulting structure can be called a tripolar vortex. On the other hand if two of the vortices are put closer to one another, and the remaining smaller vortex is put a bit further away so that it would intersect the trajectory of the dipole vortex that the former two would form, then the resulting dynamical structure is a tripolar system where a dipole vortex “collides” with a monopole at each rotation when it exchanges its weaker partner.

Finally, in a situation of oblique (non head-on) collision (i.e. the impact parameter $b \neq 0$), or near or grazing collision (i.e. $b > 2a$) where two dipoles, or a dipole and a monopole come close enough to perturb each-other’s trajectory strongly but not really collide, we either get two dipoles that are perturbed from the interaction, or merging of same sign vorticities, resulting in a larger dipole. This is also what happens when we consider a faster dipole overcoming a slower one, where the two dipoles might merge to form a larger dipole. Examples of these can be seen in sporadic turbulence simulations, reinforcing our argument that even these collisions that produce such complicated vortex merging events, eventually result in dipole vortices, locally, and therefore sporadic turbulence can be described as an ensemble of dipole vortices that move around, collide and merge.

The rest of the paper is organized as follows. Section 2 introduces the concept of sporadic turbulence using a demonstration through simple two dimensional numerical simulations. A background on basic dipole vortex solutions is given in Section 3 with the FSW vortex introduced and discussed in Section 3.1 and the Charney Hasegawa Mima modon solution recalled in section 3.2. Section 4 details the formation, dynamics and structure of dipole vortex solutions, with Section 4.1 introducing the basic setup with two Gaussian initial peaks and showing numerical examples of the dipole vortex formation from this initial state, which is studied in detail analytically in Section 4.2, showing that the final parameters of the dipole vortices can be estimated from the initial parameters of the two peaks using energy and enstrophy conservation, and then

in Section 4.3 making a detailed comparison between the analytical form of the vorticity for the FSW vortex and the numerical observation showing that these are indeed FSW vortices, and finally in 4.4 discussing the dynamics of the dipole vortices. Section 5 introduces a different family of periodic large scale solutions that can also be an element of the sporadic turbulence state as long as they remain weakly interacting with the rest of the structures. First the Stuart vortex as a simple example in Section 5.1 and a family of solutions constructed from Jacobi elliptic functions in section 5.2. The coexistence of those with dipole vortices are discussed briefly in section 5.3 leaving a detailed study of the collisions to Section 6, especially the collision between a dipole vortex and a large scale periodic flow to Section 6.1 where it was shown that a direct collision with a somewhat larger dipole vortex results in the disruption of the structure and causes the system to transit to standard 2D turbulence regime with global dual cascade. Collisions between two dipole vortices are considered in Section 6.2 with two examples where the resulting dipole is either a CL dipole or an FSW dipole depending on the distribution of vortex amplitudes. The point vortex formulation is recalled in Section 6.3, where it is pointed out that collisions between dipole vortices can be explained in terms of interactions between point vortices, and dipoles made up of two such point vortices as long as the dipoles remain far away or when they make head on collisions. As a final example, that can be understood in terms of point vortices a tripolar configuration is considered in section 6.4. Section 7 presents our conclusions.

2. Sporadic Two dimensional Turbulence

We have defined turbulence as “a duality of chaotic dynamics and self-organization of a fluid-like system across a large range of scales”. While the *multi-scale chaos* facet of this duality is what is usually studied in statistical theories that focus on the turbulent cascade, its self-organization aspect is sometimes described through the formation and the dynamics of coherent structures. A second duality in turbulence, is the one between the wave dominated weak turbulence, and the eddy dominated strong turbulence. In general, what we call turbulence is a coexistence of waves and eddies, coherent structures and multi-scale chaos. Coherent structures provide large scale gradients of velocity, density, or pressure, and those gradients can generate small scales waves and instabilities. In various limits however, the turbulence may manifest itself as purely *Kolmogorov*, or purely *wave-turbulence* etc. In the odd case of turbulence that is dominated by coherent structures - such as the dipole vortices that we discussed earlier- we get what we call the sporadic turbulence. In contrast a sporadic wave turbulence would be the wave turbulence state that can be described using a soliton gas formulation, since in a sense the structure dominated state can be thought of as a dipole vortex gas as well. Here we use the term sporadic turbulence to describe a “steady state”, which has most of its energy in coherent structures, as a result of the sparseness of its fluctuations, either because the system is in a state of transition to turbulence, or as a consequence of the initial spottiness of the turbulent kinetic energy.

Mandelbrot[11] argues using conditional probabilities that:

$$P(u(x+\ell) - u(x) \neq 0 \mid u(L) - u(0) \neq 0) \propto \left(\frac{\ell}{L}\right)^d$$

for $0 < x < x+\ell < L$, where d defines a degree of spottiness with $d = 1$ corresponding to the homogeneous case, and $d = 0$ corresponding to a single puff. One can argue that $d \lesssim 1$ corresponds to sporadic turbulence, which represents a finite number of turbulent puffs surrounded by laminar flow. Since these efforts by Mandelbrot gave rise to what we call intermittency today, we can also argue that any measure of intermittency can be used to distinguish spotty or intermittent turbulence, from homogeneous Kolmogorov like turbulence (even though Kolmogorov-like turbulence itself may have some small intermittency corrections consistent with $d \lesssim 1$). For example, we can use the behavior of structure functions $S_n(r) \propto r^{\zeta_n}$ in order to decide if a given turbulent state is sporadic or not. Since sporadic turbulence is nothing but extremely intermittent turbulence due to abundance of coherent structures, this suggests that the *intermittency is not a universal feature of incompressible two dimensional turbulence*, and one can initialize or force a turbulent system in a particular way, resulting in a qualitatively different regime of intermittency. Note that this is supported by the observations that the two dimensional turbulence is found to be intermittent in some studies[40], but not in others[5]. The sporadic turbulence state may be transient, as in the case of transition to turbulence, or decaying turbulence that is initialized to be spotty and evolving towards homogeneity. However it can also be a “steady state” if we force the system carefully to maintain the large amount of intermittency[41], to keep the system in this state. Note that similar to the transition from one or two isolated solitons, to a soliton gas and then to a state of homogeneous wave-turbulence, the exact points of transition from a single vortex to sporadic to homogeneous turbulence are rather ambiguous.

In order to study two dimensional turbulence, recall that the two dimensional Navier-Stokes system can be written as:

$$\frac{\partial}{\partial t} \nabla^2 \psi + [\psi, \nabla^2 \psi] = D_\Omega (\nabla^2 \psi) \quad (1)$$

with an additional equation for passive scalar evolution:

$$\frac{\partial}{\partial t} n + [\psi, n] = D_n (n) \quad , \quad (2)$$

where $[\psi, n]$ is the Poisson bracket, n is the passive scalar and ψ is the stream function defined in the convention, common in geophysical fluids and plasmas, so that $\Omega = \nabla^2 \psi$ is the vorticity, and D_Ω and D_n are dissipation functions for vorticity and passive scalar respectively. We have $D_\Omega (\nabla^2 \psi) = \nu \nabla^4 \psi$ from kinematic viscosity and $D_n (n) = D \nabla^2 n$ from passive scalar diffusion. When dealing with exact nonlinear solutions, like the dipole vortex solution that will be discussed in the following, we will generally consider the inviscid limit (i.e. the Euler equation limit) of the two dimensional Navier-Stokes

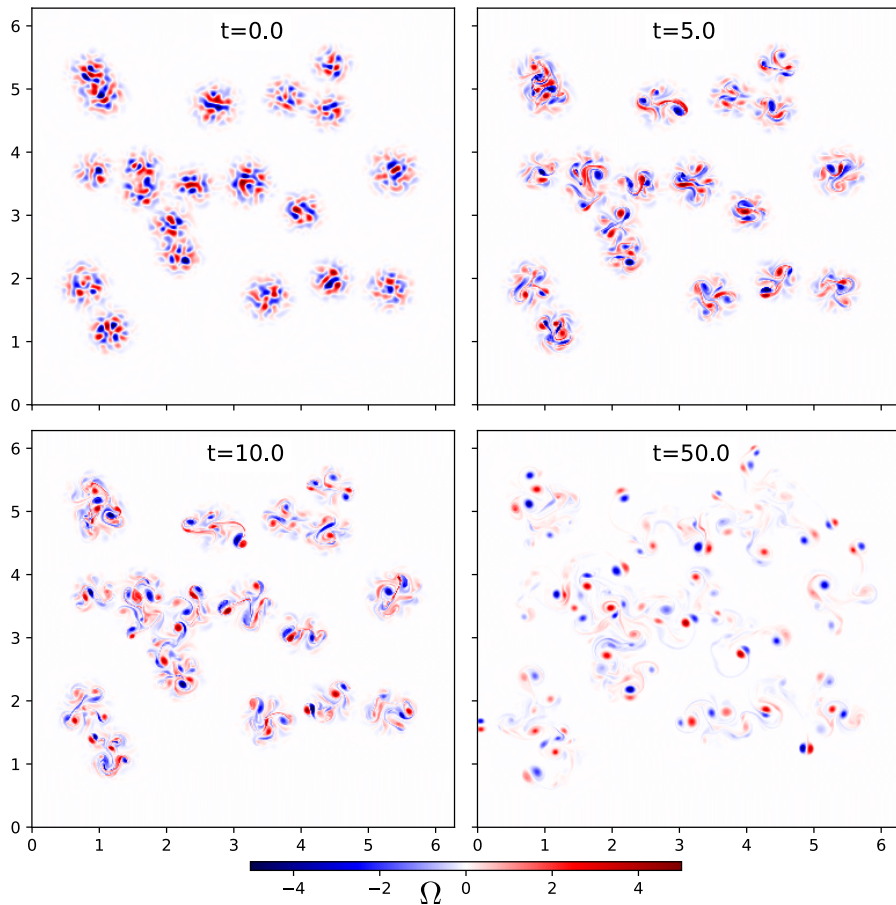


Figure 1. A decaying pseudo-spectral numerical simulation of box size $[L_x, L_y] = [2\pi, 2\pi]$, padded resolution 2048×2048 , and viscosity $\nu = 5 \times 10^{-6}$, initialized with a finite number of turbulent patches, which - through a mechanism of local selective decay- evolve to a state dominated by dipole vortices interacting with each-other, shown here as an example of sporadic two dimensional turbulence. Note that since the dipole vortices have the capability of self-propulsion, the spatial locations of active regions in the final state is different from the initial state. In fact each turbulent patch seems to generate a number of dipole vortices, which are ejected in different directions in order to conserve momentum and circulation. Two example simulations can be accessed as movie files in the online version of the paper (see Movies 1 and 2).

system. However, for the purposes of numerical studies, or more generally, we will consider small but finite viscosity (and diffusivity) in Eqns. (1) and (2).

An example of sporadic turbulence is shown in figure 1 using numerical simulations of (1), where the system is initialized in a state with a number of randomly placed turbulent patches. We see that it rapidly evolves into a state almost completely dominated by coherent structures, and in particular dipole vortices. They collide, they shed their vorticity, they interact with the tails of one another, or remnants of the initial turbulent patches, but at least for a while (these are decaying turbulence simulations), they remain in this sporadic turbulence state, dominated largely by coherent structures. We argue that this state is best described by understanding the dynamics and the

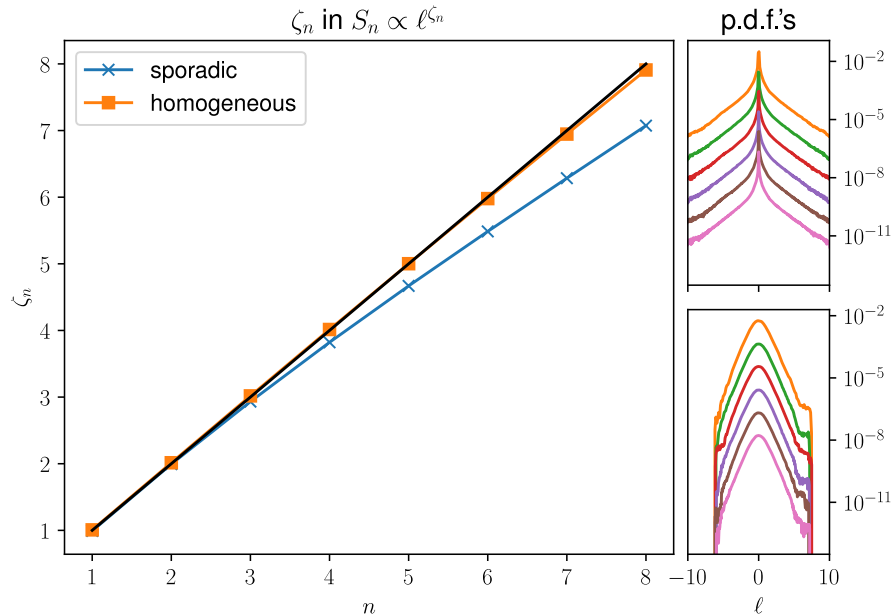


Figure 2. Intermittency of decaying sporadic vs. homogeneous turbulence as shown by the power law index ζ_n of the structure function S_n as a function of n on the left and the probability density functions (p.d.f.'s) on the right, with sporadic at the top and homogeneous at the bottom. The pdf's are computed using $\delta u(r) = \langle \hat{\mathbf{r}} \cdot [\mathbf{u}(\mathbf{x}) - \mathbf{u}(\mathbf{x} + \mathbf{r})] \rangle$ where $\mathbf{r} \equiv \ell_x \hat{\mathbf{x}} + \ell_y \hat{\mathbf{y}}$ with the pdf's for $\delta u(\ell_n)$ defined with r such that $\ell_n g^{-1/2} < r < g^{1/2} \ell_n$ and $\ell_n = \ell_0 g^n$ with $g = 1.272$, where each consecutive pdf is shifted down by a decade in order to separate them. The averages are performed both over space and time in the later stages of the simulations, and the x axes of the pdfs are normalized to $\langle \delta u_n^2 \rangle^{1/2}$ as usual. The two runs here have the same parameters as the case shown in figure 1, except with $\nu = 2 \times 10^{-6}$ and $t_{\max} = 1000$, and otherwise differ only in terms of the initial conditions. While we find that the actual form of the intermittency depends on the choice of g as well as the part of the structure function that is used for the power law fitting, we argue that the difference in intermittency between the two cases is significant and of qualitative nature.

collisions of these dipole structures. The simulations, whose results are shown in 1 are performed using a pseudo-spectral solver, using the 2/3 padding rule for anti-aliasing, with a padded resolution of 2048×2048 and using regular viscosity with $\nu = 5 \times 10^{-6}$ on a periodic box of size $(L_x, L_y) = (2\pi, 2\pi)$. The initial condition consists of a random phase broadband signal, which can be written in Fourier space as:

$$\tilde{\psi}_{\mathbf{k}}^{(0)} = A e^{-\mathbf{k}^2/2\sigma_k^2 + 2\pi i \tilde{\xi}_{\mathbf{k}}}, \quad (3)$$

where $\tilde{\xi}_{\mathbf{k}}$ is a random variable, $A = 10^3$ (with the convention that only the inverse transform is normalized), and $\sigma_k = 30$. The initial condition $\psi_0(x, y)$ is then obtained by computing the inverse fast Fourier transform of Eqn. (3). and multiplying it by an envelope function that consists of 20 randomly positioned (avoiding the edge regions) Gaussian peaks of random amplitudes between 0 and 0.2 and random widths between 0.02 – 0.04.

We can also see that each turbulent patch generates a number of dipole vortices, which are ejected in different directions in order to conserve momentum and circulation. The intermittency of decaying sporadic vs. homogeneous turbulence are compared in figure 2 using the power law indices ζ_n of the structure function S_n as a function of n and the probability density functions of velocity deviations $\delta u(r) = \langle \hat{\mathbf{r}} \cdot [\mathbf{u}(\mathbf{x}) - \mathbf{u}(\mathbf{x} + \mathbf{r})] \rangle$ where $\mathbf{r} \equiv \ell_x \hat{\mathbf{x}} + \ell_y \hat{\mathbf{y}}$ with the pdf's for $\delta u(\ell_n)$ defined with r such that $\ell_n g^{-1/2} < r \leq g^{1/2} \ell_n$ on a logarithmic partition $\ell_n = \ell_0 g^n$ with $g = \sqrt{\frac{1+\sqrt{5}}{2}} \approx 1.272$. The detailed form of the intermittency correction in decaying turbulence simulations depend on the time range that is considered for the averaging, the choice of g as well as the part of the structure function that is used for the power law fitting. However the difference of intermittency between the two cases is significant suggesting a qualitatively different character.

The formation of a dipole vortex from a turbulent patch was studied earlier, but with an initial setup having finite net momentum, so that the whole patch combines neatly to form a single dipole vortex[42]. Here we show that even in the general case of zero (or near-zero, random initial) momentum, a strong initial turbulent patch generates a finite number of dipole vortices, that are ejected in opposite directions in order to conserve momentum. We will discuss this process below in some detail with the simpler example of two Gaussian peaks.

Note also that in a state dominated by coherent nonlinear structures, such as dipole vortices, nonlinear terms vanish unless there is an interaction. A dipole vortex that is moving in isolation, has no nonlinearity acting on it, and therefore generates no turbulent flux in k -space, neither forward, nor inverse. Thus, sporadic turbulence is likely to generate much less turbulent flux, and it does so only through interactions among coherent structures, whose movement is the only mechanism by which they would collide. This makes the dipole vortex more important, since while a monopolar vortex, would sit around, and in a sporadic turbulence setting (where the structures are isolated), not initiate a collision, a dipole vortex will move around and therefore is more likely to make collisions.

Finally, looking at the transition to homogeneous turbulence, it can be argued that as one decreases intermittency, the system becomes more and more crowded with coherent structures making more and more frequent collisions, and they have to find ways of packing and squeezing themselves against one another, transitioning from a gas-like state of coherent structures (i.e. if we consider the example in figure 1 as a gas of dipole vortices) to a liquid-like state and eventually as they move towards a state of constant interaction -similar to a condensate- such that in the final state, turbulence would be statistically homogeneous. This suggests that there may be a measure of the turbulence "state" such as its temperature, which would somehow determine its state. However the transition between sporadic and homogeneous turbulence is unlikely to involve sudden changes as in the case of phase transitions. As an interesting example, it seems that for whatever reason, the two dimensional turbulence discussed in Ref. 40

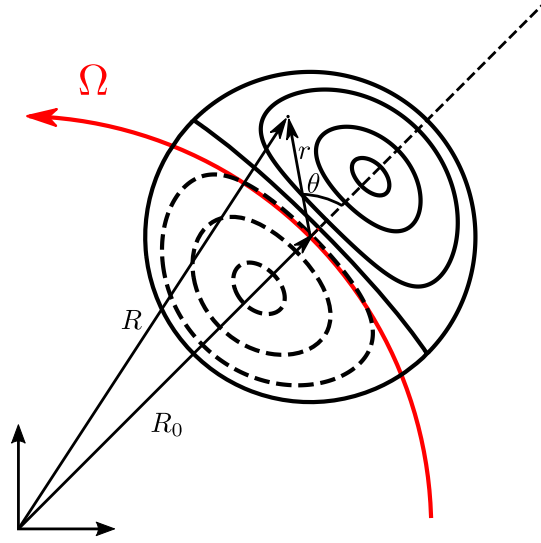


Figure 3. The FSW dipole vortex.

display features of a crowd of dipoles packed against one another, and therefore, appears to be not completely homogeneous, maybe yielding a larger intermittency as a result.

3. Basic Dipole Vortex Solutions:

3.1. FSW Rotating Dipole Vortex Solution

Following Ref. 35, we consider an asymmetric dipole that follows a phase locked circular orbit around the origin. Using polar coordinates around its center of rotation (i.e. R and φ), and switching to a rotating frame $\varphi = \varphi' - \omega t$, we get:

$$\left(\frac{\partial}{\partial t} - \omega \frac{\partial}{\partial \varphi} \right) \nabla^2 \psi + [\psi, \nabla^2 \psi] = 0, \quad (4)$$

which means that if

$$\left[\psi - \frac{1}{2} \omega R^2, \nabla^2 \psi \right] = 0 \quad (5)$$

we have a stationary solution in the rotating frame. Defining a as the radius of the dipole vortex, switching to the polar coordinates defined with respect to the center of the dipole (i.e. r and θ , see figure 3) and using the law of cosines:

$$R^2 = R_0^2 + r^2 + 2rR_0 \cos \theta \quad (6)$$

where R_0 is the distance between the center of rotation and the center of the dipole vortex, the relation (5), becomes:

$$\left[\psi - \frac{1}{2} \omega r^2 - \omega r R_0 \cos \theta, \nabla^2 \psi \right] = 0. \quad (7)$$

Setting $\nabla^2\psi = 0$ in the exterior of the vortex (i.e. $r > a$, where a is the vortex radius), we can write:

$$\psi = \omega a^2 \left(\frac{R_0}{r} \cos \theta + B \ln \frac{r}{a} \right) \quad (8)$$

so that $\psi'(a) = -\omega a^2/2$ is independent of θ , where $\psi' \equiv \psi - \frac{1}{2}\omega r^2 - \omega r R_0 \cos \theta$. In the interior we have:

$$\nabla^2\psi' + 2\omega = -k^2 \left[\psi' + \frac{1}{2}\omega a^2 \right] \quad (9)$$

so that enforcing continuity at $r = a$, we get

$$\psi' = -\frac{2\omega R_0 J_1(kr)}{kJ_0(ka)} \cos \theta + \frac{2\omega}{k^2} \left(\frac{J_0(kr)}{J_0(ka)} - 1 \right) - \frac{1}{2}\omega a^2 \quad (10)$$

and $B = 1$ in (8), so that for ψ , we can write:‡

$$\psi = \begin{cases} ua \left(\frac{r}{a} - \frac{2J_1(kr)}{kaJ_0(ka)} \right) \cos \theta + \frac{2u\epsilon}{k^2 a} \left(\frac{J_0(kr)}{J_0(ka)} - 1 \right) + \frac{\epsilon u}{2a} (r^2 - a^2) & r \leq a \\ ua \left(\frac{a}{r} \cos \theta + \epsilon \ln \frac{r}{a} \right) & r > a \end{cases} \quad (11)$$

where $\epsilon \equiv a/R_0$ is the aspect ratio and $u \equiv \omega R_0$ is the linear velocity. The form of (11) provides a convenient general form for the dipole vortex since as the curvature goes to zero (i.e. $\epsilon \rightarrow 0$), we get the usual Chaplygin-Lamb vortex propagating in a straight line.

The dipole vortex in (11) is written in the rotating frame, using cylindrical coordinates defined with respect to the center of the vortex. If the center of rotation is $\mathbf{r}_0 = (x_0, y_0)$ instead of the origin, r and θ in (11) become

$$r \equiv \sqrt{(\delta x - R_0 \cos \omega t)^2 + (\delta y - R_0 \sin \omega t)^2},$$

$$\theta \equiv \arctan \left(\frac{\delta y - R_0 \sin \omega t}{\delta x - R_0 \cos \omega t} \right) - \omega t,$$

where $\delta x = x - x_0$, $\delta y = y - y_0$, written explicitly in laboratory coordinates using the parameters x_0, y_0 which represent the position of the center of rotation, R_0 and a , which represent the radius of curvature of its orbit and the radius of the dipole vortex, and u or Ω which represent its linear velocity or rotation rate. If we imagine a dipole vortex in a slowly changing background as it would be the case in a real turbulent environment, one would argue that these parameters would be slowly changing functions of time and space. In this sense, the dipole vortex solution of Eqn. (11) can be thought of representing a general curved trajectory, with a local curvature determined by the local value of ϵ .

It is also possible to replace the Eqn. (9), with a nonlinear relation between $\nabla^2\psi'$ and ψ' . A polynomial form can for the relation between vorticity and stream function,

‡ In order to compare with the the unnumbered equation at the bottom of Page 255 of Ref. 35 one has to use $u \rightarrow -u$ and $\theta \rightarrow \pi/2 - \theta$

results in a slightly modified dipole vortex that remains localized and stable [43]. Other nonlinear forms of the relation results in different kinds of nonlinear vortex solutions. Some of these solutions can be chosen to represent the large scale, periodic background state as will be discussed in section 5.

Finally, from the point of view of plasma turbulence, for example considering the Hasegawa-Wakatani equations[44], the vorticity equation decouples from the density equation when the electron mobility is small, and then we can have these dipole vortex solutions for the electrostatic potential, which plays the role of the stream function in plasma turbulence. In this limit, the density equation needs to be solved as a passive scalar equation with a background density gradient, with no back-reaction to the electrostatic potential. On the other hand in the large electron mobility limit, density gets pegged to the electrostatic potential and we get the Charney-Hasegawa-Mima system[45, 46], which can be written as:

$$\partial_t (\psi - \nabla^2 \psi) + \beta \partial_y \psi = [\psi, \nabla^2 \psi] \quad (12)$$

in the inviscid limit, and if the gradients from the dipole vortex are larger than background gradient (i.e. the β -effect, where β is the gradient of planetary vorticity in the geophysical fluid dynamics case, or the background density in the plasma case), the latter can be considered as a perturbation on the solution given above. This is actually the case of Ref. 35. However if this is not the case, the dipole vortex solution for the Charney-Hasegawa-Mima becomes a particular case of the general solution, which can only propagate in y direction.

3.2. The Charney-Hasegawa-Mima Modon Solution:

Considering the Charney-Hasegawa-Mima system in Eqn. (12) and assuming a stationary solution moving in the y direction with the velocity u , we get:

$$[\psi', \nabla^2 \psi' + (\beta - u)x] = 0, \quad (13)$$

where $\psi' = \psi - ux$, which is the basis of the dipole vortex solution, with

$$\nabla^2 \psi' + (\beta - u)r \cos \theta = \begin{cases} -k^2 \psi' & r \leq a \\ +p^2 \psi' & r > a \end{cases}, \quad (14)$$

where k and p are constants to be determined from matching conditions below. The simplest such solution is probably the one given by $\eta = 0$. If we impose $\psi'(a) = 0$, we get:

$$\psi'(r, \theta) = ua \cos \theta \times \begin{cases} \frac{p^2}{k^2} \left(\frac{r}{a} - \frac{J_1(kr)}{J_1(ka)} \right) & r \leq a \\ \left(\frac{K_1(pr)}{K_1(pa)} - \frac{r}{a} \right) & r > a \end{cases} \quad (15)$$

together with the condition that $\psi(r \rightarrow \infty) \rightarrow 0$, so that:

$$p^2 = 1 - \frac{\kappa}{u} \quad (16)$$

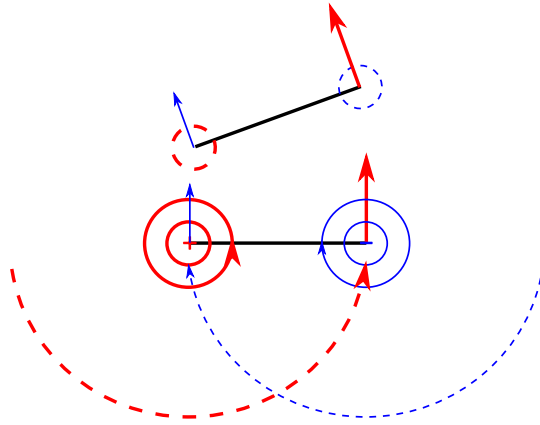


Figure 4. Interaction of two unequal monopolar vortices of opposite signs. A stronger positive vorticity vortex on the left, results in a counter-clockwise rotation as it drags the weaker vortex along its streamlines. If the weaker vortex was very small it would be advected by the flow of the larger vortex like a passive scalar. Note that the initial part of the cartoon also works for understanding the effect of a sheared flow on the dipole vortex.

with $u \geq \kappa$ in order to have a $p \in \mathbb{R}$. The electrostatic potential in the moving frame (i.e. with $r = \sqrt{x^2 - (y - ut)^2}$ and $\theta = \arctan[(y - ut)/x]$) can then be written as:

$$\psi(r, \theta) = ua \cos \theta \times \begin{cases} \frac{p^2}{k^2} \left(\frac{r}{a} \left(1 + \frac{k^2}{p^2} \right) - \frac{J_1(kr)}{J_1(ka)} \right) & r \leq a \\ \frac{K_1(pr)}{K_1(pa)} & r > a \end{cases}, \quad (17)$$

where k is to be determined from the continuity of the radial derivative at $r = a$, or:

$$\frac{K_2(pa)}{K_1(pa)} + \frac{p J_2(ka)}{k J_1(ka)} = 0. \quad (18)$$

Note that the CHM modon solution as given in (17) propagates only in the y direction and has a non-zero vorticity outside, even though since $\psi(r \rightarrow \infty) \rightarrow 0$, has zero vorticity far away from it. It is clear that for relatively weak β , we have the FSW dipole, slightly modified by the β effect, whereas for strong β , we get the CHM modon discussed above. One needs to resort to numerics for the details of the transition from one to the other for moderate β with non-zero ϵ . Similarly the case of Hasegawa-Wakatani turbulence with arbitrary adiabaticity parameter seems to be an interesting case out of the scope of the current work, where some form of dipole vortex can be observed without an obvious simple analytical solution.

4. Formation and Structure of the Dipole Vortex

4.1. Dipole Vortex Formation

A monopole vortex is probably the simplest solution of the Euler equations. It consists of a cylindrically symmetric solution, which naturally makes the nonlinear term vanish

since the velocity in such a configuration is purely in the poloidal direction whereas the gradient of vorticity is purely in the radial direction resulting in the vanishing of their scalar product.

In general, we observe, in accordance with Ref. 27, that if we put two monopole vortices of opposite vorticities close to one another, they form a dipole vortex that moves together in the direction of the flow between the two vortices. Consider, for example, a positive vorticity vortex on the left, which has a counter clockwise flow and a negative vorticity vortex on the right, which has a clockwise flow. The counter-clockwise flow of the left vortex advects the right vortex upwards, while the clockwise flow of the right vortex advects the left vortex upwards. Hence, if the two vorticities are of equal magnitude, they move upwards by the same amount and keep moving upwards as the line between the two vortices remains horizontal. In contrast if one of the vorticities is bigger, the upward motion imposed by its flow will be larger, and therefore the smaller vortex will move upwards faster. This will cause the line between the two vortices to tilt with respect to the horizontal, and since in the next step the advection will be perpendicular to this tilted line, the resulting trajectory will be a rotation around the larger vortex (see figure 4). Note that in the example given above if the left vortex is larger (this means we have a net positive vorticity), the resulting dipole vortex will start by moving upwards and tilt towards the left, to end up rotating in the counter clockwise direction as implied by the net excess of positive vorticity. In contrast if we exchange the two vorticities, (i.e. have a larger positive vortex on the right), the dipole will start by moving down but tilt towards the larger vortex on the right, to end up rotating, again, in the counter-clockwise direction. Obviously if we make the negative vorticity vortex larger, the rotation will be in the clockwise direction. In both cases the larger vorticity stays in the inside part of the rotating dipole vortex. In other words, when the initial amplitudes of the two peaks are the same, the resulting dipole vortex has zero net vorticity and therefore corresponds to the $\varepsilon = 0$ case of the FSW vortex, or a simple Chaplygin-Lamb dipole vortex moving only in y direction. In contrast, when the two peaks have different amplitudes, the resulting dipole vortex has a net vorticity and therefore rotates in the direction implied by the excess vorticity as in the general ε FSW solution, discussed in Section 3.1.

The details of the interaction between the two vortices (i.e. whether they attract each other or not) depends on the radial profile of the peaks that one uses to initialize the dipole vortex. In particular if we start with a Gaussian form for the stream function, the two vortices end up attracting each other and forming a rather tight dipole vortex as can be seen in figures 5 and 6. On the other hand, if we choose a Gaussian form for the vorticity, the two vortices remain relatively separated. It is also worth mentioning that when we choose a Gaussian form for the stream function, the vorticity (i.e. Laplacian of a Gaussian) is positive in the core and negative in the periphery. When two such vortices interact, the core vorticities stick together forming the main dipole, while the rim vorticities of opposite sign also come together and form a secondary dipole vortex of opposite polarity that is weaker, slower and more diffuse than the primary dipole

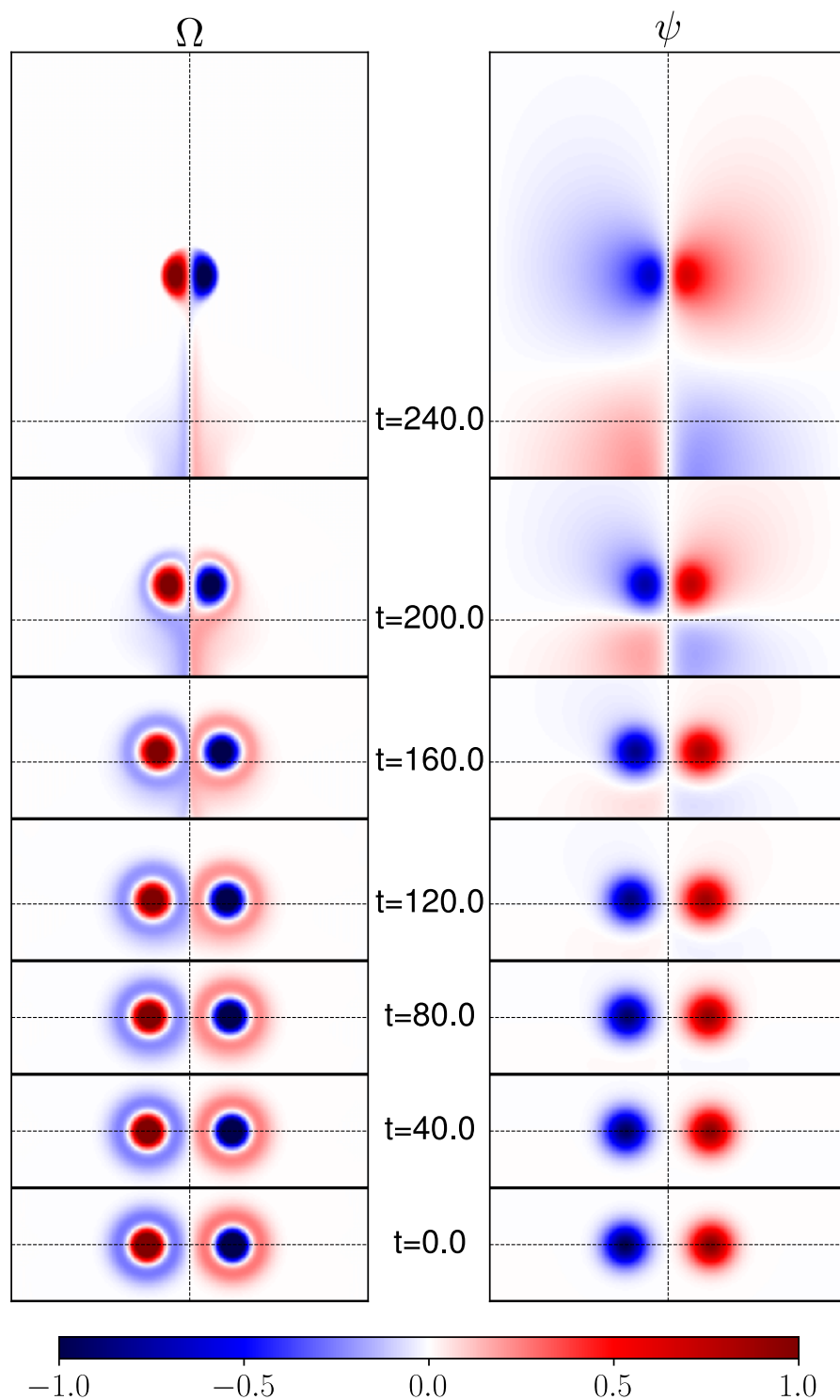


Figure 5. Formation of a dipole vortex, from the interaction of two gaussian stream function peaks of the same amplitude that are $d = 6$ apart initially. The two peak vorticities of opposite sign attract each-other in order to form a dipole vortex structure moving upwards as the rim vorticities of opposite sign of each peak is ejected downwards forming another more diffuse dipole moving downwards (we only see its tail in these plots). The resulting dipole is practically equivalent to the Chaplygin-Lamb dipole. The movie version can be accessed in the online version of the paper (see Movie 3).

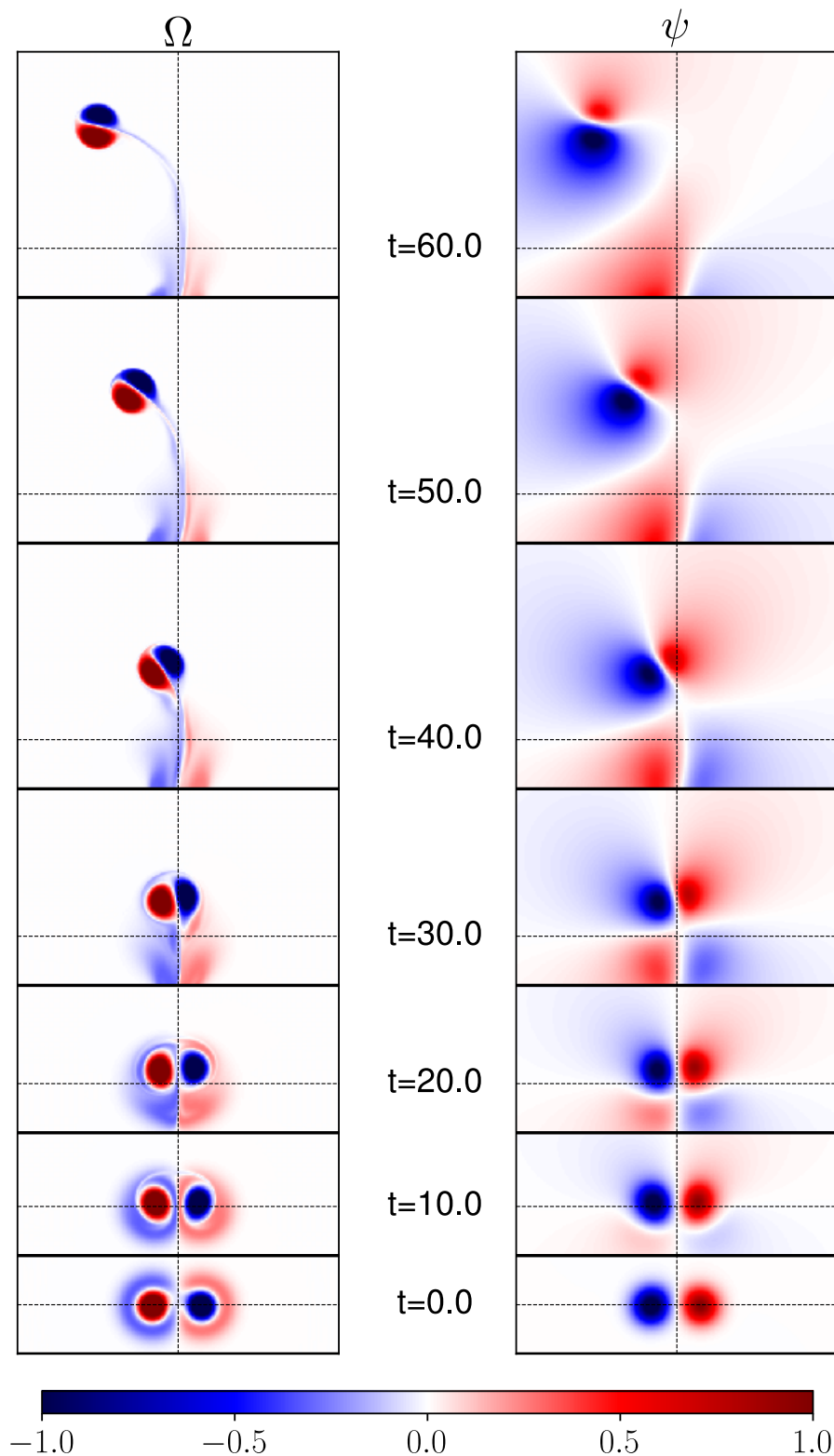


Figure 6. Formation of a rotating dipole vortex, from the interaction of two gaussian stream function peaks of different amplitudes that are $d = 4$ apart initially. The amplitude of the peak on the left is 1.2 times that of the one the right. Note that as the peak vorticities form the primary dipole vortex rotating in counter clock-wise direction, the rim vorticities form a secondary dipole that is weaker, slower and more diffuse, rotating in the clock-wise direction. Here we mostly only see its tail. The movie version can be accessed in the online version of the paper (see Movie 4).

vortex, moving (and rotating if vorticities are imbalanced) in the opposite direction.

4.2. Estimating final dipole vortex state from initial data

The two dimensional Navier-Stokes system conserves energy

$$E \equiv -\frac{1}{2} \int \psi \Omega dS, \quad (19)$$

which is positive since the vorticity $\Omega \equiv \nabla^2 \psi$ and $\psi \nabla^2 \psi = \nabla \cdot (\psi \nabla \psi) - (\nabla \psi)^2$, and the enstrophy:

$$W \equiv \frac{1}{2} \int \Omega^2 dS, \quad (20)$$

up to small viscous effects. In order to analyze the initial condition of two Gaussian stream functions, which we argue provides a simplified example for more general cases, at $t = 0$, we have:

$$\psi(0) = \psi_+(0) + \psi_-(0),$$

where

$$\psi_{\pm}(0) = A_{\pm} e^{-\left[\frac{(x \pm d)^2 + y^2}{2\sigma^2}\right]}$$

with d sufficiently large that it does not substantially deform the $\Omega = 0$ separatrices, but small enough that the outer rims of the two Gaussians touch each-other in order to allow interaction. Using $\Omega = \nabla^2 \Phi$, we have $\Omega(0) = \Omega_+(0) + \Omega_-(0)$, with:

$$\Omega_{\pm}(0) = \frac{A_{\pm}}{\sigma^4} \left[(x \pm d)^2 + y^2 - 2\sigma^2 \right] e^{-\left[\frac{(x \pm d)^2 + y^2}{2\sigma^2}\right]}.$$

In order to use conservation of energy and enstrophy between this initial state and the final state with the dipole vortex, we compute the Laplacian of Eqn. (11) in order to write

$$\Omega = \begin{cases} \frac{2ukJ_1(kr)}{J_0(ka)} \cos \theta - \frac{2u\epsilon}{a} \left(\frac{J_0(kr)}{J_0(ka)} - 1 \right) & r \leq a \\ 0 & r > a \end{cases}. \quad (21)$$

We can then write

$$E(0) = -\frac{1}{2} \int \psi(0) \Omega(0) dx dy \approx \frac{\pi}{2} (A_+^2 + A_-^2)$$

$$W(0) = \frac{1}{2} \int \Omega^2(0) dx dy \approx \pi \frac{(A_+^2 + A_-^2)}{\sigma^2},$$

where we have neglected the interaction terms, which would be multiplied by coefficients of the form e^{-d^2/σ^2} . These would indeed be negligible for the numerical example in figure 5 with $d = 3$ and $\sigma = 1$. Computing the Energy and Enstrophy for the FSW dipole vortex, we get:

$$E = \pi u^2 \left(2a^2 + \frac{\epsilon^2}{k^2} \left[6 + \frac{k^2 a^2}{4} \right] \right)$$

and

$$W = \pi u^2 (k^2 a^2 + 4\epsilon^2) .$$

In the limit $\epsilon \rightarrow 0$, and $A_- = -A_+ = A$, conservation of energy gives

$$E = E(0) \Rightarrow u = \frac{A}{\sqrt{2}a} \quad (22)$$

and using conservation of enstrophy and Eqn. (22), we get:

$$W = W(0) \Rightarrow a = \frac{j_{11}}{2}\sigma, \quad (23)$$

which gives the radius of the final dipole vortex in terms of the width σ of the initial Gaussian peaks ($j_{11}/2 \approx 1.92$). Going back to (22), we find:

$$u = \frac{\sqrt{A_+^2 + A_-^2}}{\sigma j_{11}}, \quad (24)$$

in terms of the initial parameters. For the example in figure (5), we get $u \approx 0.37$, which is very close to what is observed in numerical simulations, where u is expected to be a bit smaller anyway due to viscosity.

In order to solve for ϵ as well we need an additional conserved quantity so that we can have three equations and three unknowns (u , a and ϵ). For this, we consider circulation, or the net vorticity, which can be written as:

$$M \equiv \int \Omega ds .$$

However for the two Gaussian initial condition, even when the two peaks are not equal, this vanishes exactly when we integrate over the full domain. However since it is somewhat apparent from the numerical simulations that it is the two circles inside the separatrices that combine to form the final dipole, we consider the circulation only from the regions inside the two separatrices. We can write that as:

$$M_{r < 2\sqrt{\sigma}}(0) = -4\pi (A_+ + A_-) ,$$

which vanishes for $A_- = -A_+$ as expected, but is finite otherwise. Similarly the circulation of the final dipole vortex can be computed by integrating Eqn. (21), which gives:

$$M = 2\pi u \epsilon a .$$

Now the three equations that needs to be solved are:

$$u^2 a^2 \left(2 + \frac{\epsilon^2}{j_{11}^2} \left[6 + \frac{j_{11}^2}{4} \right] \right) = \frac{1}{2} (A_+^2 + A_-^2) \quad (25)$$

$$u^2 (j_{11}^2 + 4\epsilon^2) = \frac{(A_+^2 + A_-^2)}{\sigma^2} \quad (26)$$

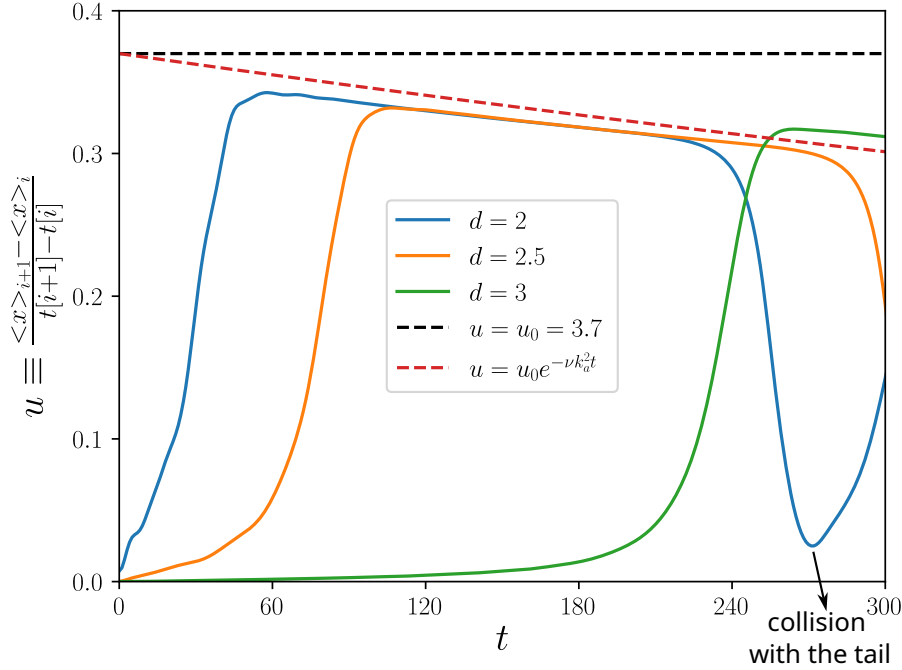


Figure 7. The trajectories as computed from Eqn. (32) for three different values of the half distance d between the two initial Gaussian peaks. We see that $d = 2$ saturates at around $t = 58$, $d = 2.5$ at around $t = 107$ and $d = 3.0$ around $t = 264$, consistent with a scaling of the form $(t_s - t_{s0}) \propto (d - d_0)^2$. The slowly decaying form suggested by Eqn. (33), with $u_0 \approx 0.37$ as estimated by (24) seems to be a reasonable approximation to the trajectory once the dipole is formed, at least until it makes a collision with its own tail because of periodic boundary conditions.

and

$$2(A_+ + A_-) = -u\epsilon a, \quad (27)$$

which can be solved as

$$u = \sqrt{\frac{(A_+^2 + A_-^2)}{\sigma^2 (j_{11}^2 + 4\epsilon^2)}} \quad (28)$$

$$a = \frac{\sigma j_{11}}{2} \sqrt{\frac{j_{11}^2 + 4\epsilon^2}{j_{11}^2 + \epsilon^2 (3 + j_{11}^2/8)}}, \quad (29)$$

where

$$\epsilon = \frac{2(A_+ + A_-)}{\sqrt{(A_+^2 + A_-^2) - 4(A_+ + A_-)^2 (3/j_{11}^2 + 1/8)}} \quad (30)$$

in practice, for $A_{\pm} = \Delta A/2 \pm A$, as long as $\Delta A/2 \ll A$, we get $\epsilon \ll 1$, and so that we can drop ϵ from Eqns. (28) and (29), and use:

$$\epsilon \approx \sqrt{2} \frac{\Delta A}{A}. \quad (31)$$

Note that for the example for the case in figure 6, we have $A = 1.1$ and $\Delta A = 0.2$ which gives $\epsilon \approx -0.25$ from either (30) or (31), and using $a = 1.91$ as before we get

$R_0 \approx 7.64$. Note that while the a expands slowly and u slows down with finite viscosity, and thus these inviscid estimates for a and u are lower and upper bounds respectively, the radius of curvature R_0 is not affected as much by the viscosity and appears to be a better estimate. This means that in the finite viscosity state both ϵ and a increase similarly in order to keep R_0 relatively constant. See Section 4.3 for a detailed fit of the numerical observation and the analytical form of the FSW vortex.

Finally, it is interesting to note that the parameter d (the distance between the initial Gaussian peaks) does not play a role in the final state, but it determines how fast the dipole vortex is formed. In order to see this we have performed a series of reruns of the scenario in figure 5, with a higher resolution elongated box ($N_x \times N_y = 1024 \times 4096$, with $L_x \times L_y = 8\pi, 32\pi$ and $\nu = 10^{-4}$), so that the interaction with the tail is delayed, and where we put the initial perturbation at the bottom at $y_0 = L_y/8$, computing the position of the dipole using a weighted average of the form

$$\langle y \rangle = \frac{\sum_{i,j} |\Omega(x_i, y_j)|^{2n} y_j}{\sum_{i,j} |\Omega(x_i, y_j)|^{2n}} \quad (32)$$

with $n = 4$ in order to drop the influence of the secondary dipole vortex (i.e. the tail) whose amplitude is generally much smaller. Then, we compute the velocity u using finite difference of $\langle y \rangle$ in time using $u \equiv \frac{\langle y \rangle_{i+1} - \langle y \rangle_i}{t_{i+1} - t_i}$, which we can plot as a function of time $u(t)$ as a sort of trajectory (e.g. see figure 7). For this case, we expect it to accelerate and then saturate to a constant velocity u which is estimated by Eqn. 24. We can also estimate the decay rate for velocity as

$$u(t) \approx u e^{-\nu k_a^2 t}, \quad (33)$$

where k_a corresponds to $k_a = 2\pi/\lambda_a$, with $\lambda_a = 2aj_{01}/j_{11}$ is the distance between the two maxima of the vorticity profile of the dipole vortex. The time to saturation as a function of d follows a diffusive scaling (i.e. $t_d \propto d^2$ as can be observed in figure 7).

For the case with finite net circulation, the weighted position follows a circular orbit that has two components $\langle \mathbf{x} \rangle = \hat{\mathbf{x}} \langle x \rangle + \hat{\mathbf{y}} \langle y \rangle$ and the velocity and acceleration can be computed as $|u| = \sqrt{\langle \dot{x} \rangle^2 + \langle \dot{y} \rangle^2}$ and $|\dot{u}| = \sqrt{\langle \ddot{x} \rangle^2 + \langle \ddot{y} \rangle^2}$, which can be computed numerically using finite differences in time. The radius of curvature can then be computed numerically from the Newton's law as:

$$|\dot{u}| = \Omega^2 R_0 = \frac{|u|^2}{R_0} \Rightarrow R_0 = \frac{|\dot{u}|}{|u|^2}. \quad (34)$$

Note that this ignores the interaction with the tail, and is therefore bound to result in errors in computation of both $|u|$ and $|\dot{u}|$ as well as in the way we compute R_0 (i.e. assuming that we have a purely centrifugal motion). Nonetheless if we compute $|u|$, $|\dot{u}|$ and R_0 from finite difference formulas on $\langle x \rangle$ and $\langle y \rangle$ and (34) also averaging over time after the dipole is established, for the example for the case shown in figure 6, instead of performing a detailed parameter fit as will be presented in section 4.3,

we get $|u| \approx 0.3$, $|\dot{u}| \approx 0.012$ and $R_0 \approx 7.4$ (averaging each quantity separately from $t = [80, 450]$). These are consistent with $u \approx 0.37$ and $R_0 \approx 7.64$ as predicted above, slowed down due to interactions with the tail. In fact if we average over $t \in [40, 120]$ which roughly corresponds to the first rotation we get $|u| \approx 0.33$, whereas if we average over $t = [400, 480]$ we find $|u| \approx 0.28$, which decreases in steps each time the primary dipole collides or passes near the secondary one.

Application of the use of energy and enstrophy conservation for arbitrary initial data, in order to determine the final dipole vortex parameters is also rather straightforward, especially if we know that there is only one dipole vortex that forms out of a given initial data represented by a perturbation with total enstrophy W_0 and total energy E_0 :

$$u \approx \frac{\sqrt{W_0}}{\sqrt{\pi}j_{11}} \text{ and } a \approx \frac{j_{11}\sqrt{E_0}}{\sqrt{2}\sqrt{W_0}}.$$

However the identification of a separatrix in order to use the conservation of circulation for estimating ϵ from arbitrary initial data is considerably more complicated and requires numerical analysis. Alternatively one can imagine decomposing the initial vorticity distribution into wavelets of the form of Laplacians of Gaussians, identifying the vortex pairs that are close enough to interact along the lines of Ref. 14, and apply the methodology given above to estimate the parameters u , a and ϵ for each pair. Limitations of this approach becomes evident when the initial data starts to have overlapping interactions with multiple dipoles forming out of multiple initial peak pairs all close to one another. One can speculate that such a complex initial state could be studied as a formation of multiple dipoles followed by a collision of those as will be discussed in Section 6.2.

4.3. Detailed Structure of the Dipole Vortex

Even though we have shown that a dipole vortex is formed when two Gaussian stream function vortices are put somewhat close together, there is no guarantee that these are the FSW dipole vortices that we discussed in section 3.1. In order to see whether or not they are, we need to study the detailed radial and poloidal structure of the resulting dipole vortices[47].

Consider the dipole vortex of figure 6, which rotates around a center of rotation, at the time $t = 200$, roughly a quarter of the way into its second rotation. Focusing on the dipole vortex, choosing its approximate center as the origin and extrapolating $\Phi(x, y) \rightarrow \Phi(r, \theta)$ into a grid of polar and radial coordinates defined with respect to this origin, we can get its detailed radial and poloidal structure (see figure 8). In order to compare this to the exact solution, we rewrite (21) as:

$$\Omega = \begin{cases} \frac{2ukJ_1(kr)}{J_0(ka)} \cos(\theta - \theta_0) - \frac{2u\epsilon}{a} \left(\frac{J_0(kr)}{J_0(ka)} - 1 \right) & r \leq a \\ 0 & r > a \end{cases}, \quad (35)$$

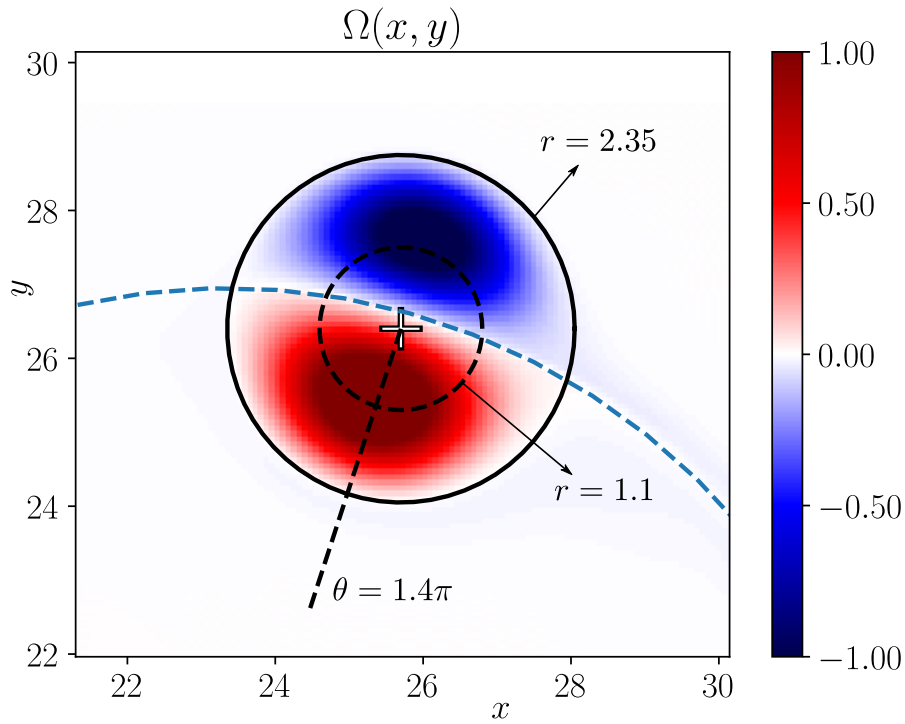


Figure 8. The dipole vortex of figure 6 at $t = 200$, roughly quarter of the way into its second rotation. Dark dashed lines show the cross-sections at $r = 1.1$ and $\theta = 1.4\pi$ that are shown in figure 9. Note that the origin is chosen by hand as $(x_0, y_0) = (25.7, 26.4)$.

where $a = j_{1,1}/k$. The analytical expression of vorticity in FSW dipole as given in Eqn. (35) has three independent parameters. For example, we can choose k , u and ϵ as independent parameters, and the observed features such as a and R_0 can be written in terms of these three variables. However, we can equally choose a, u and ϵ or a, u and R_0 as the independent parameters, and the remaining two as observed features. It is interesting to observe that the functional dependence of Eqn. (35) on r and θ is spot on with the naturally generated dipole from two Gaussian stream-function vortices as shown in figure 8. We can also verify these features from the numerical values of the coefficients that we obtain by performing a least square fit of the data to the analytical form of Eqn. (35), resulting in $\theta_0 = -1.6\pi$, $k = 1.68$, $\epsilon = 0.3$ and $u = 0.25$, which in turn gives $a = 2.3$ and $R_0 = 7.6$. The a and R_0 that is plotted in figure 8 is actually $R_0 = 9.1$, however this difference is probably due to the fact that the dipole vortex does not follow an exactly circular orbit due to its interactions with its own tail. In contrast $a = 2.3$ is indeed very close to the $a = 2.35$ that is plotted in figure 8, even though the k that is suggested in figure 9 gives a smaller radius. Note that the apparent radius of the dipole may indeed get slightly larger due to viscosity in numerical simulations. The inviscid analytical estimates from the initial data for this case from Eqns. (23), (24) and (31) are $u \approx 0.37$, $a = 1.91$ and $R_0 \approx 7.64$, respectively. Increasing the resolution in order to be able to decrease viscosity and looking at the state immediately after the formation of the dipole does indeed reduce the difference between the estimate and the

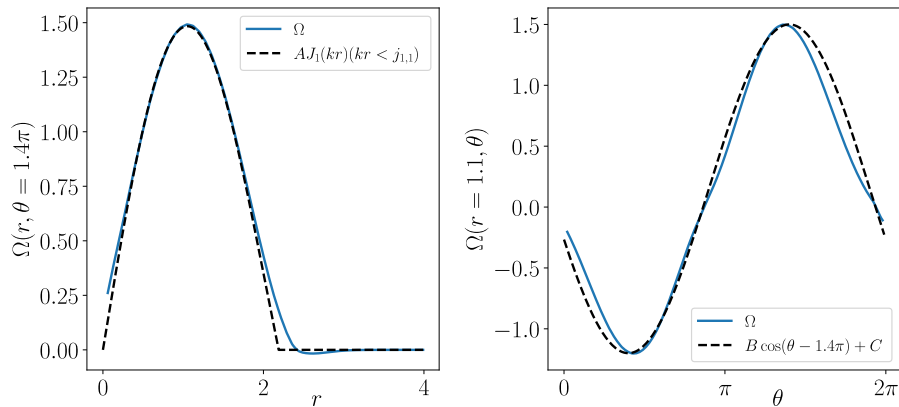


Figure 9. The radial and the poloidal profiles of the dipole vortex of Figure 8. The solid lines show the numerical forms, whereas the dashed lines are the analytical expressions. The dashed line on the left is $\Omega(r) = AJ_1(kr)$, with $A = 2.55$ and $k = 1.75$, up to the first zero of $J_1(kr)$ (i.e. $kr < j_{1,1}$) and zero afterwards, whereas the one on the right is $\Omega(\theta) = C \cos(\theta - 1.4\pi) + D$, with $C = 1.35$ and $D = 0.15$.

observation. Note that the discrepancy in velocity is also partly from the fact that at $t = 200$, the dipole has already interacted once with its tail, which also slows it down considerably.

In short, a careful comparison of the detailed structure of the generated dipole vortex to the analytical expression in Eqn. (35) shows undoubtedly that it corresponds to the FSW dipole, slightly modified due to viscosity and with a modulated trajectory because of its interaction with its own tail. This suggests that not only that the dipole vortex is an important nonlinear feature of the sporadic turbulence state, but also specifically that the FSW dipole vortex is an important nonlinear solution of the two dimensional Navier-Stokes system, since a random initial distribution of positive and negative Gaussian vortices of different amplitudes would form an ensemble of these robust nonlinear structures, and interact only as a result of collisions or near collisions among them. Also, as discussed earlier in Section 5.3, since these structures are localized, they can survive in the presence of large scale vortex chains or zonal flow patterns as long as they remain in parts of the large scale solution where the vorticity gradients are small. However, these structures would nonetheless interact with a nontrivial large scale flow by colliding with its shear layers, where the vorticity gradients may be significant. In order to discuss such an interaction, we consider a class of large scale periodic solutions in Section 5, and interaction between a dipole vortex and such a solution in Section 6.1.

4.4. Dynamics of the Dipole Vortex

Dipole vortex, even in its approximate form as in the general case of its realization in the presence of background turbulence, usually has a well defined separatrix that contains it. Since the system conserves energy and enstrophy as discussed in section 4.2, up to small viscous effects and vortex shedding in its approximate form, the integrals in Eqns. (19-20) can be limited to inside of the separatrix since for the exact solution, we

have $\Omega = 0$ outside. This allows one to define the energy and the enstrophy as *intrinsic properties* of a dipole vortex, which are conserved apart from collisions between vortices, or interactions between a vortex and a background nonlinear structure like a shear layer.

We can divide the FSW dipole vortex into its monopolar and dipolar components:

$$\Omega = \Omega_0(r) + \Omega_1(r, \theta) , \quad (36)$$

where

$$\Omega_0(r) = -\frac{2u\epsilon}{a} \left(\frac{J_0(kr)}{J_0(ka)} - 1 \right) \quad (37)$$

$$\Omega_1(r, \theta) = \frac{2ukJ_1(kr)}{J_0(ka)} \cos \theta \quad (38)$$

so that the full streamline can be written as;

$$\psi = \bar{\psi}(r, \theta) + \psi_0(r) + \psi_1(r, \theta) , \quad (39)$$

where

$$\bar{\psi} = ur \cos \theta + \frac{\epsilon u}{2a} (r^2 - a^2) \quad (40)$$

$$\psi_0(r) = \frac{2u\epsilon}{k^2 a} \left(\frac{J_0(kr)}{J_0(ka)} - 1 \right) \quad (41)$$

and

$$\psi_1(r, \theta) = -\frac{2uJ_1(kr)}{kJ_0(ka)} \cos \theta . \quad (42)$$

Note that both ψ_0 and ψ_1 vanish on the separatrix, while $\bar{\psi}(a) = ua \cos \theta$. With these, we can write the evolution equations for the monopole and dipole components of vorticity as:

$$\frac{\partial \Omega_0}{\partial t} = -u \sin \theta \frac{\partial}{\partial r} \Omega_0 \quad (43)$$

$$\frac{\partial \Omega_1}{\partial t} = -\left(\frac{u}{r} \cos \theta + \frac{\epsilon u}{a} \right) \frac{\partial}{\partial \theta} \Omega_1 - u \sin \theta \frac{\partial}{\partial r} \Omega_1 . \quad (44)$$

As discussed in some detail in Section 7.3 of Batchelor's book (also see [48]), the net vorticity, or circulation:

$$M \equiv \int \Omega dS = \int \Omega_0 dS = 2\pi u \epsilon a , \quad (45)$$

which vanishes for a symmetric dipole but is non-zero for an asymmetric one plays the role of effective mass for the evolution of the vortex. It is worth mentioning that the position weighted by the isotropic vorticity component Ω_0 has its center at the center of the FSW vortex. That is:

$$\langle \mathbf{x} \rangle_{\Omega_0} \equiv \frac{\int \Omega_0 \mathbf{x} dS}{\int \Omega_0 dS} = \mathbf{R}_0 , \quad (46)$$

where $\mathbf{x} = [R_0 \cos \phi + r \cos(\theta + \phi), R_0 \sin \phi + r \sin(\theta + \phi)]$ is the position from the center of rotation as shown in figure 3. Note that using only Ω_0 to weight the position,

velocity and acceleration of the vortex makes it more practical, since Ω_0 is symmetric and isotropic around its central point. One can write the time rate of change of this averaged position as:

$$\mathbf{u} \equiv \frac{d \langle \mathbf{x} \rangle_{\Omega_0}}{dt} = \frac{\int \mathbf{x} \frac{\partial}{\partial t} \Omega_0 dS}{\int \Omega_0 dS} = \frac{\hat{\mathbf{z}} \times \mathbf{R}_0}{R_0} u, \quad (47)$$

which can be derived by substituting Eqn. (43) into Eqn. (47), and finally the time rate of change of this average velocity can be written in the form:

$$\frac{d}{dt} \mathbf{u} = \boldsymbol{\omega} \times (\boldsymbol{\omega} \times \mathbf{R}_0), \quad (48)$$

where $\boldsymbol{\omega} = \omega \hat{\mathbf{z}}$ is the rotation frequency. We can interpret the RHS of Eqn. (48) as a centripetal force. The form of Eqn. (48) can be derived by writing:

$$\frac{\int \partial_t (\partial_t \Omega_0) \mathbf{x} dS}{\int \Omega_0 dS} \rightarrow \frac{d}{dt} \mathbf{u}$$

and assuming that the vortex is advected by $\hat{\mathbf{z}} \times \nabla \bar{\psi}$ as defined in Eqn. (40), which is justified by the observation that the interaction terms between Ω_1 and Ω_0 gets cancelled when we put everything together. Representing the position, the velocity and the acceleration of the dipole vortex using Ω_0 means that when Ω_0 is zero, we can not define an acceleration. Instead, we can define the net dipole moment using Ω_1 :

$$\begin{aligned} \mathbf{p} &= \int \Omega_1 (\mathbf{x} - \mathbf{R}_0) dS \\ &= \int (\mathbf{x} - \mathbf{R}_0) \frac{2ukJ_1(kr)}{J_0(ka)} \cos \theta dS \\ &= -2\pi ua^2 \frac{\mathbf{R}_0}{R_0} = -M\mathbf{R}_0, \end{aligned}$$

which is in the direction opposite to \mathbf{R}_0 . Similarly we can write:

$$\begin{aligned} \frac{d\mathbf{p}}{dt} &= \int (\partial_t \Omega_1) (\mathbf{x} - \mathbf{R}_0) dS = \frac{\hat{\mathbf{z}} \times \mathbf{p}}{R_0} \\ &= -M\mathbf{u} \end{aligned}$$

for the rate of change of the dipole moment, which is in a direction perpendicular to itself consistent with rotation. Note that a symmetric dipole has no mass (e.g. like a photon), and therefore it propagates in a straight line with constant polarization. Note that the same approach applies to the case of Charney-Hasegawa-Mima modon when the background gradient length scale is small compared to the size of the dipole vortex[48].

5. Periodic Large Scale Nonlinear Solutions

Two localized vortices of opposite signs attract one another and eventually form a dipole vortex. Unless the two initial peaks are of the same magnitude, the dipole vortex that

forms, ends up having a net vorticity and therefore have a tendency to follow a circular path. This makes the dipole vortex solution given in Eqn. (11) rather ubiquitous. This solution also applies to the Charney-Hasegawa-Mima system if the background gradients are weak, or the modon solution of Eqn. 17 can be used in the opposite case. However all of these solutions rely on a linear relation between the vorticity and the stream-function in a bounded circular region. Nonlinear versions based on a polynomial relation between the vorticity and the stream function can be developed and observed in numerical simulations as generalizations [43]. However, a whole different class of solutions of the two dimensional Euler system exists, and can be relevant depending on the boundary conditions, and other constraints that the vorticity evolution has to respect as large scale, periodic solutions. Here we consider some interesting cases.

5.1. The Stuart Vortex

Consider a stationary solution of the form[36]:

$$\psi = \ln [\cosh kx - \varepsilon \cos ky] , \quad (49)$$

which is periodic in y but converges to a straight line in x , and satisfies the relation:

$$\nabla^2 \psi = k^2 (1 - \varepsilon^2) e^{-2\psi} . \quad (50)$$

It is important to note that the solution as written here is neither periodic, nor localized in the x direction. As a result it would make sense only as a local or a partial solution in the periodic box.

5.2. Solutions based on Jacobi elliptic functions

The Stuart vortex solution of Eqn. (49) can also be written as: $\psi = \ln [\cosh^2 k'x - \varepsilon \cos^2 k'y - (1 - \varepsilon)/2]$ with $k' = k/2$. Both the cosine and the cosine hyperbolic that appear in it are limits of the Jacobi elliptic functions. Thus, a reasonable generalization may be written in the form [49, 50] :

$$\psi = \ln (Af^2(x) + Bg^2(y) + C) , \quad (51)$$

where $f(x)$ and $g(y)$ are one of the Jacobi elliptic functions[51]. For example choosing $f(x) = \text{cn}(kx|m)$ and $g(y) = \text{cn}(k'y|m')$, gives $A = mk^2$, $B = m'k'^2$ and $C = ((1 - 2m)k^2 + (1 - 2m')k'^2)/3$, with

$$\gamma \equiv \frac{k'}{k} = \frac{(1 - m + m^2)^{1/4}}{(1 - m' + m'^2)^{1/4}} , \quad (52)$$

and a Laplacian

$$\nabla^2 \psi = -2e^\psi + \chi e^{-2\psi} , \quad (53)$$

where

$$\chi = \frac{4k^6}{27} \left[(2m-1)(m-2)(m+1) + (2m'-1)(m'-2)(m'+1)\gamma^6 \right]. \quad (54)$$

Some examples of this type of solution are shown in figure 10. Note that this solution is periodic in both x and y with the periods $\ell_x = 2K(m)/k$ and $\ell_y = 2K(m')/k'$ respectively [i.e. $\psi(x + \ell_x, y + \ell_y) = \psi(x + \ell_x, y) = \psi(x, y + \ell_y) = \psi(x, y)$]. In order for such a solution to be realized in a periodic box, one should have a box size that is a multiple of these periods.

There are two other independent solutions as discussed in Ref. 50 (with some typos), which are independent of the first one. First one of these solutions can be written by choosing $g(y) = \text{dc}(k'y|m')$ where $\text{dc}(u) \equiv \text{dn}(u)/\text{cn}(u)$. This choice gives $B = -k'^2$ and $C = ((1-2m)k^2 + (1+m')k'^2)/3$, with the same value for A and the relations (52-54). Finally we can also pick both $f(x) = \text{dc}(k'y|m')$ and $g(y) = \text{dc}(k'y|m')$, which would give $A = -k^2$, $B = -k'^2$ and $C = ((1+m)k^2 + (1+m')k'^2)/3$. These three solutions cover a whole class of solutions of the form (51) with f and g being any one of the Jacobi elliptic functions, since shifting by half a period and/or using the well known relations between squares of the Jacobi elliptic functions, one can go from one function to another.

We also used this opportunity to verify these solutions numerically in the presence of small viscosity. We have observed that apart from the $m = m' = 1/2$ case which caused some sort of singularity in the initial condition (but for example the case $m = 0.49$, $m = 0.5$ works), the general family of solutions where m and m' is varied between 0 and 0.5 were numerically realizable, and were exact solutions of the 2D Navier-Stokes equations up to (small) dissipation. These solutions can for example be used for testing the numerical accuracy of the underlying solver. However, since our focus here is the dipole vortex, we consider these solutions only as a nontrivial large scale background flow, on which the former may propagate. While it is clear that in principle there is no superposition of nonlinear solutions, in practice one may consider coexistence of different nonlinear solutions, and see what happens. The result of one such interaction is shown in Section 6.1.

5.3. Coexistence of Nonlinear Solutions

The Stuart vortex solution of Eqn. (49) for large x asymptotes to $\psi \approx kx$. This means that one can put a dipole vortex solution in this region without having any interaction with the vortex sheet in the middle. For example if we let:

$$\Phi = \ln [\cosh kx - \varepsilon \cos ky] + \Phi_D^a(\mathbf{x} - \mathbf{x}_0(t)),$$

where $\Phi_D^a(\mathbf{x} - \mathbf{x}_0(t))$ denotes a dipole vortex solution localized within a radius a and following a trajectory denoted by $\mathbf{x}_0(t)$, where $kx_0(t) \gg 1 \gg ka$, so that the center of

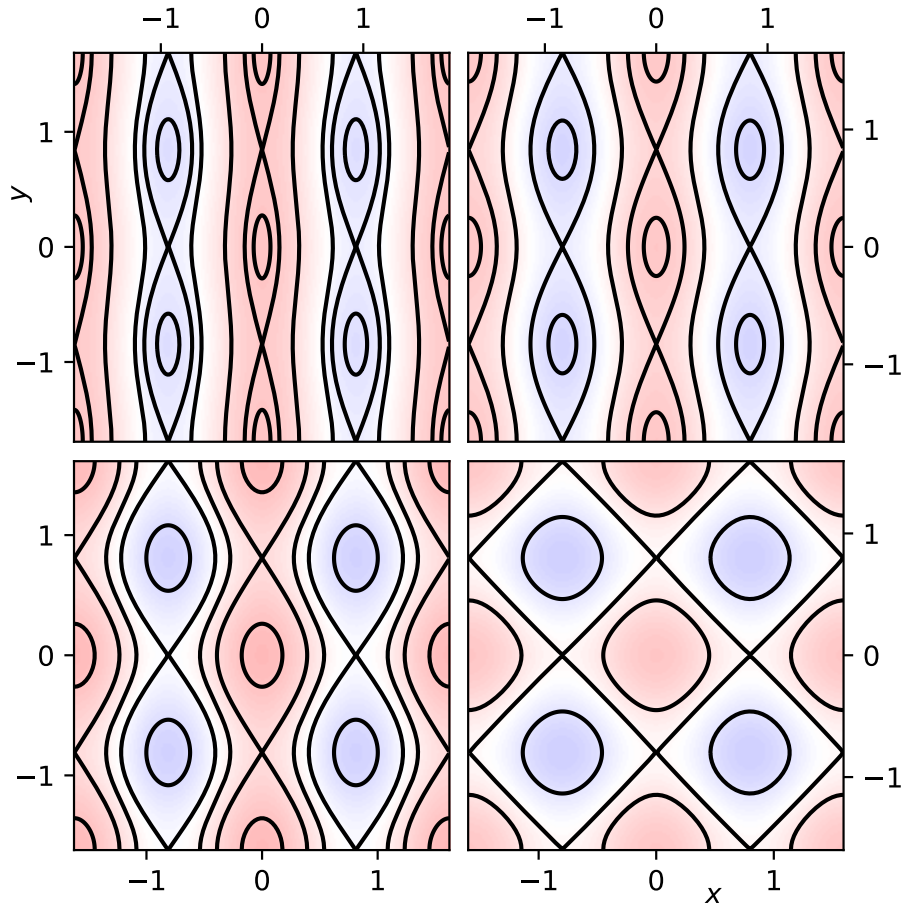


Figure 10. Contours of ψ of Eqn. (51) with $f(x) = \text{cn}(kx|m)$ and $g(y) = \text{cn}(\gamma ky|m')$ with $k = 1.0$, γ , given by Eqn. (52), and $(m, m') = (1/2, 1/16)$, $(1/4, 1/16)$, $(1/8, 1/16)$ and $(1/16, 1/16)$ from top left to bottom right respectively. The colors are only indicative of the topology of the solution since the solution is meaningful up to an additive constant anyway and its amplitude changes as we change m . Note that the range of x and y values are chosen to guarantee periodicity.

the dipole vortex is always far away from the central part of the Stuart vortex solution, we have a new solution where the two nonlinear solutions coexist together. It is clear that

$$[\psi, \nabla^2 \psi] = 0$$

everywhere, where $\nabla^2 \psi$ vanishes (or is a constant), and in the region where $\ln[\cosh kx - \varepsilon \cos ky] \approx kx$, the dipole vortex solution is only modified slightly, by defining $\mathbf{u}' = (\mathbf{u} + k\hat{\mathbf{y}})$ as an effective vertical propagation velocity. This is basically the flow at infinity from the Stuart vortex solution advecting the dipole vortex without causing any distortion. Similarly, one should in principle consider the effect of the flow at infinity from the dipole vortex solution on the central part of the Stuart vortex, but the dipole vortex solution has zero flow as $x \rightarrow \infty$, so that is negligible.

This approach works more generally in the sense that as long as the vorticity in a given region from one solution is negligible or constant, one can add another solution

with local nonzero vorticity in that region, but has zero vorticity outside of it (e.g. a dipole vortex), and the effect of one on the other will be simple advection. This means that more general solutions can be constructed as a patchwork of different nonlinear solutions as long as there is no overlap of vorticities. We discuss this here, because this is, in some sense, the basis of sporadic turbulence state. Each solution, be it a dipole vortex, a monopole vortex or a chain of vortices like the Stuart vortex, or a sheared flow, can coexist and interact only weakly through occasional collisions. And when there is overlap, as in the case of a dipole vortex plunging into a shear layer, if the shear is strong enough with respect to the dipole the large scale flow would likely shear apart the smaller structure, leading to a new, probably a slightly different large scale solution with additional incoherent fluctuations that result from the breaking up of the small scale eddy. However when the incoming dipole is large enough, the large scale periodic solutions such as those given in Eqn. (51) can be disturbed sufficiently that they become unstable and transform the nature of the flow. This kind of state then evolves to more standard homogeneous states of two dimensional turbulence, with a global dual cascade.

It may nonetheless be speculated that, for a given system with additional linear physics such as two dimensional turbulence with rotation, or as in drift wave turbulence, the abundance of some large scale structures such as zonal flows may be explained by their robustness to such incursions by dipole vortices, which are the dominant coherent structures in sporadic turbulence.

6. Vortex Interactions

Starting with a random initial distribution of a small number of high intensity turbulent patches, we observe that the system evolves to a state in which the dipole vortices are the dominant structures, together with other structures such monopoles, tripoles, narrow shear layers or larger scale overall circulation. The dipole vortices in such a state, move around under the weak influence of one another until the point that they collide either with another dipole or some other object. As such most of the self propulsion in this kind of sporadic two dimensional turbulence, -different from advection by the large scale flow shearing and rotation- is due in one form or another, to dipole vortices.

6.1. Interaction with a background flow

Considering a standard FSW vortex advected in a large scale flow that is constant or sufficiently slowly varying, a co-moving frame can be defined as

$$\mathbf{x}' = \mathbf{x} - (\mathbf{U} + \mathbf{u}) t ,$$

where \mathbf{U} is the external fluid velocity and $\mathbf{u} = \omega \hat{\mathbf{z}} \times \mathbf{R}_0$ is the internal velocity corresponding to the rotation (or the propagation in a straight line for the case $\epsilon \rightarrow 0$) of the dipole in the moving frame. Writing the Euler equation in such a frame we get back Eqn. (4), and can follow the derivation in Section 3.1 in order to obtain the usual

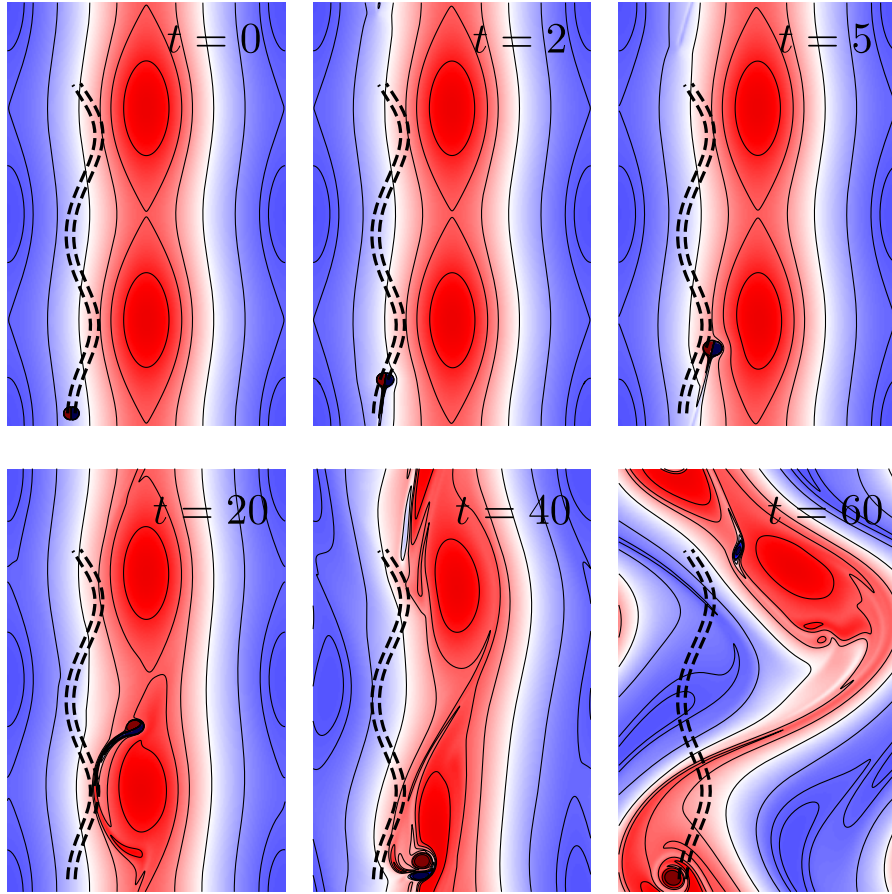


Figure 11. The snapshots of the interaction between a dipole vortex with $a = 0.1$, $u = 0.5$, and $\epsilon = 0$ and the exact solution with two Jacobi elliptic functions from Figure 10 with $m = 1/2$, $m' = 1/16$. The dashed lines are the trajectories (up to $t = 20$) of the two point vortices that correspond approximately to the initial dipole vortex, evolving in the initial background flow field, kept constant in time. The domain in these figures is $x \in [0, L_x]$ where $L_x = 2K(m) \approx 3.71$ and $y \in [0, L_y]$ where $L_y = 4K(m')/\gamma \approx 6.76$ with γ given in Eqn. (52), and the initial position of the dipole vortex is $x_0 = L_x/2 - 1 \approx 0.85$ and $y_0 = 0.2$. The movie version can be accessed in the online version of the paper (see Movie 5).

FSW solution with \mathbf{u} defined as the velocity in the moving frame this time, rather than the lab frame. Note that while the velocity in the lab frame is $\mathbf{U} + \mathbf{u}$, the alignment of the dipole is such that its dipole moment is still perpendicular to \mathbf{u} as implied by the form of Eqn. (11). This results for example for the CL limit, in a dipole that is tilted with respect to its direction of propagation in the lab frame.

The effect of weak shear is more interesting[52] and can be understood at a basic level by considering the two lobes of vorticity of the dipole as point vortices that are advected by the flow resulting in a curved motion of the dipole vortex in the same spirit as in figure 4. And as in that case, if we start with an initial state of two Gaussian vortices, separated by a distance d , the actions of the two monopoles of opposite signs on one another causes both to move upwards, at the same time approaching each other

to form a dipole vortex. However if the sheared flow is such that the one on the right is advected faster, than the resulting dipole vortex is tilted to the left resulting in a curved path. Note that because of lack of symmetry in a sheared flow, the dipole vortex generated from two Gaussian stream function vortices of equal amplitude separated by a distance d , may acquire a small net vorticity during its formation. It may also shed vorticity in a non-symmetric way along its trajectory, and if the angle of propagation and the direction of shear are not nearly parallel, this may cause the two poles being driven away from each other, resulting in the disintegration of the dipole vortex.

Moreover, the back-reaction of the dipole on the background flow is also important and unless there is substantial scale separation, it must be taken into account. In order to study these phenomena we take one of the solutions presented in Section 5, in particular the first one in figure 10, with $m = 1/2$ and $m' = 1/16$, in a box of size $L_x = \ell_x$ and $L_y = 2\ell_y$ as a nontrivial large scale flow profile, with large scale shear, that is perfectly stable in the absence of any perturbations. This means that the large scale solution, by itself, can be integrated for very long time in 2D Navier-Stokes and decays extremely slowly. We then introduce an exact CL dipole vortex at the bottom of the box roughly halfway left of the center (i.e. $x_0 = L_x/2 - 1$ and $y_0 = 0.2$) using the exact solution and applying a Gaussian filter in order to smooth out the discontinuity of the exact solution. The result of the numerical integration is presented in Figure 11, where the evolution of the dipole vortex, together with the background flow profile given by the large scale periodic solution is shown. Initially the dipole follows a path implied by the two point vortex approximation that is discussed in more detail in section 6.3, but as it sheds some of its vorticity along its path, which appears as a tail in Figure 11 its form starts deviating from the initial approximation before it starts substantially modifying the background flow itself. Eventually the small scale perturbations caused by the passage and presence of the dipole vortex structure and its tail, starts perturbing the steady background vorticity profile and the system evolves towards an unstable dynamical state as shown in the last plot of figure 11.

We see that the dipole vortex eventually destabilizes this particular solution based on Jacobi elliptic functions, which is taken to represent a steady large scale flow pattern. We can devise the perturbation to be less damaging by choosing its amplitude, location and initial direction of propagation. However it is clear that a steady large scale flow pattern that can not endure the passage of a dipole vortex, which is the dominant structure in sporadic turbulence, is unlikely to occur naturally in conditions that favor sporadic turbulence state. One can speculate nonetheless that, if there are classes of large scale structures that are robust to such incursions by dipole vortices, they are likely to be abundant in the sporadic turbulence state. For example in particular problem in plasma or geophysics, the zonal flows may be able to absorb dipole vortices, without becoming unstable themselves. This would explain why in such a system we would see zonal flows and not other large scale flow patterns as more or less steady state solutions.

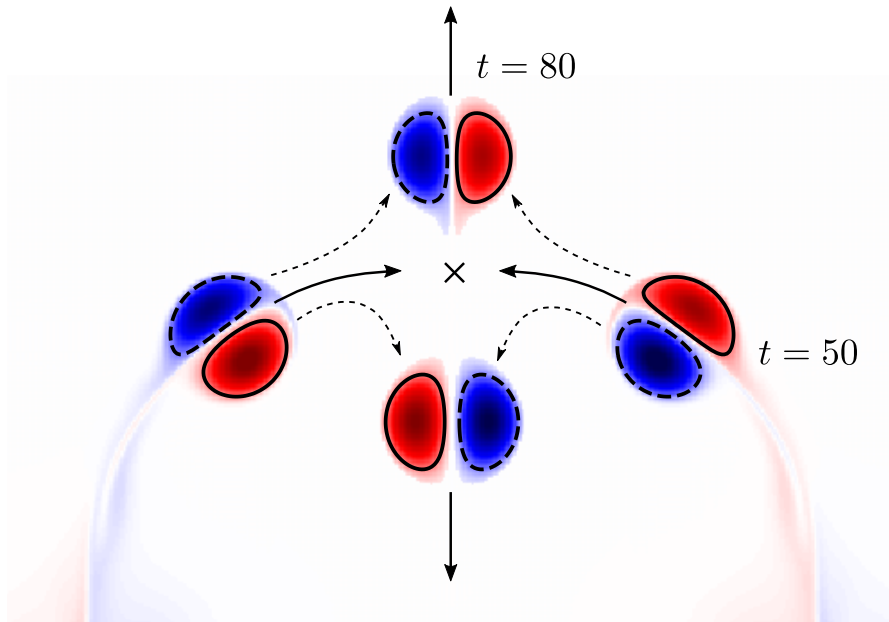


Figure 12. Collision between two FSW dipole vortices, that rotate in opposite directions, where the inner lobes are initialized to be 1.2 times larger than the outer lobes. At $t = 50$, two rotating FSW dipoles are moving towards one another, and at $t = 80$ they exchange partners and each dipole becomes symmetric (i.e. CL dipoles) and therefore move vertically away from one another. Note that the lower dipole in the final state contains the two larger lobes, and therefore moves slightly faster than the other one. The movie version can be accessed in the online version of the paper (see Movie 6).

6.2. Collisions between two Rotating Dipole Vortices

Collision of two CL vortices has been studied in some detail in various numerical configurations[53, 54, 55] and in experiment[56] in the past. However, for FSW vortices, since these move in circular trajectories, and if we allow the system to form the dipole vortex solutions as discussed in Section 4.1, instead of using the exact solutions as the initial conditions, it becomes slightly more complicated to setup an initial state that will eventually result in a collision. Since the radius of the circular trajectory of the resulting dipole vortex of section 4.3 was $R_0 \approx 9.1$, we have initialized the two pairs of Gaussians of opposite sign in such a way as the two dipole vortices that are formed, have a distance $R \approx 10$ initially. The left dipole vortex is chosen as to have an excess positive vorticity so that it would turn in clockwise direction, whereas the dipole vortex on the right is chosen to have an excess negative vorticity (of the same amount) so that it would rotate in the counter clockwise direction with the same speed, so that we would approximately -but not necessarily exactly- have a head on collision (see figure 12). As they encounter, the collision happens, by two dipoles exchanging their partners and forming symmetric (i.e. CL) dipole vortices that move vertically in opposite directions to one another, very similar to the result shown in Ref. 57. In the final state, the larger symmetric dipole that is made up of the two inner lobes of the initial asymmetric

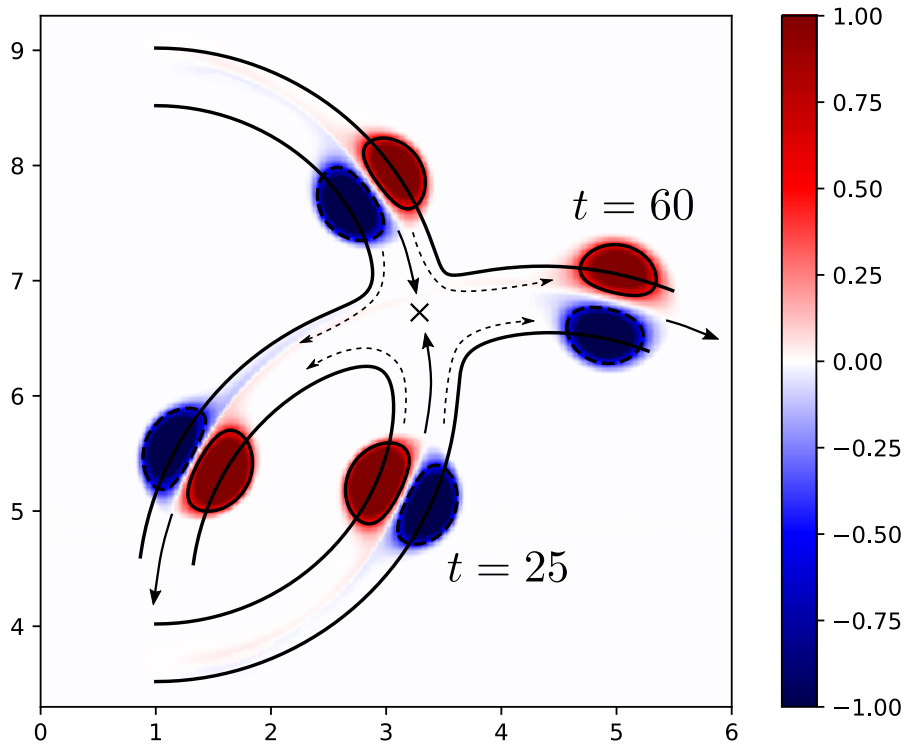


Figure 13. Collision between two FSW vortices rotating in opposite directions. The two vortices are initialized using the exact form in Eqn. 35, with $a = 0.5$, $\epsilon = 0.2$ and $u_1 = 0.12$ and $u_2 = 0.1$. The solid lines represent the time integration of the equivalent point vortices as defined by Eqns. (59), (60), (65) and (66). The point vortices appear to be slightly ahead, possibly due to the small amount of viscosity. The movie version can be accessed in the online version of the paper (see Movie 7).

dipoles, move down slightly faster than the smaller symmetric dipole that moves up. In fact since the boundary conditions are periodic, the two CL dipoles cross the periodic boundary, collide again, and are transformed back into the original FSW dipoles before the collision, but rotating around different centers.

Initializing the system with two pairs of Gaussians, as discussed above, allows it to form two dipole vortices that collide in their circular orbits, naturally. But it also generates secondary dipoles moving in the opposite direction from the outer rims of the Gaussian stream functions, where the vorticity is opposite sign to the peak, and therefore the resulting trajectories are not exactly circular. In contrast, if we want to control, precisely, the parameters of the two dipole vortices involved in the collision, say a_1 , u_1 , ϵ_1 , a_2 , u_2 and ϵ_2 corresponding to the parameters of Eqn. 11 for the two vortices, it makes more sense to use the exact form of the vorticity as given in Eqn. 35 as the initial condition (applying a Gaussian filter in order to smooth out the initial discontinuity). This way, we can define an initial state with two well localized dipole-vortices that follow a known circular path, and we can construct collisions exactly as we want. For example a head on collision of two FSW dipole vortices of equal $\epsilon_1 = \epsilon_2 = \epsilon$ and $a_1 = a_2 = a$, but different u 's, after the collision results in two new FSW vortices following circular orbits

of their own as shown in figure 13. Note that the the circular orbits after such a collision neither have the same radii nor the same angular speeds, and even the sizes of the two dipoles are different, but the detailed trajectories can be computed using a point vortex approximation, where the initial vorticity can be approximated using a collection of point vortices of different signs, whose later evolution can be using Helmholtz's formulation.

6.3. Point Vortex Approximation

As mentioned in previous section, many of the interactions discussed previously, as well as the tripolar configuration that is discussed in section 6.4 can be understood in terms of interactions between point vortices. While this is somewhat elementary, in order to study the limitations of such a formulation we visit the details of the point vortex formulation and compare with numerical results. It is found that head on collisions, tripolar configurations as well as non-interacting dipoles can be described by such a formulation, however close or grazing collisions, collisions of FSW vortices at an angle, or the interactions between dipole vortices and a nontrivial large scale flow can not be described by the point vortex formulation. We also discuss the point vortex approximation of FSW vortices, which we believe were not explicitly discussed in earlier works even though equivalent configurations were.

Nonetheless, a simple estimation of the resulting trajectories can be made by approximating each FSW dipole vortex as consisting of two point vortices[37, 38]. We can write a general two point vortex dipole as:

$$\Omega_p = \gamma_+ \delta(z - z_+(t)) + \gamma_- \delta(z - z_-(t)) ,$$

where $z_{\pm}(t) \equiv x_{\pm}(t) + iy_{\pm}(t)$ are the position vectors written as complex variables and we can define $\gamma_+ = \kappa + \lambda$ and $\gamma_- = -\kappa + \lambda$ so that $\lambda = \frac{\gamma_+ + \gamma_-}{2}$ is the asymmetric and $\kappa = \frac{\gamma_+ - \gamma_-}{2}$ is the symmetric part of the vorticity profile. For a general system of n point vortices with complex positions z_i and circulations γ_i , the evolution equations can be written as:

$$\frac{dz_i}{dt} = \sum_{j \neq i} \frac{i\gamma_j}{2\pi(z_i^* - z_j^*)} + i\partial\psi_b(z_i(t), t) ,$$

where $\partial\psi_b \equiv \partial_x\psi_b + i\partial_y\psi_b$ is the background flow represented as $\mathbf{v}_b = \hat{\mathbf{z}} \times \nabla\psi_b = -\partial_y\psi_b\hat{\mathbf{x}} + \partial_x\psi_b\hat{\mathbf{y}} = -\partial_y\psi_b + i\partial_x\psi_b = i(\partial_x\psi_b + i\partial_y\psi_b)$. It is easy to see that for $N = 2$ and with $\gamma_1 = \gamma_+$ and $\gamma_2 = \gamma_-$ with $\psi_b = 0$, we get a solution of the form $z_{\pm} = Z_0 + (R_0 \mp b_{\pm})e^{i\omega t}$, where:

$$\omega = \frac{\gamma_+ + \gamma_-}{2\pi d'^2} \quad (55)$$

with b_{\pm} being the initial distance between the center of the dipole to each vortex so that $d' = b_+ + b_-$ is the distance between the two vortices. Recall that by choosing x in the direction opposite to the dipole moment of the vortex in accordance with the usual convention in this paper, the relevant moments of an FSW vortex can be written as:

$$\int \Omega d^2x = 2\pi u a \epsilon \quad (56)$$

$$\int \Omega (x - R_0) = -2\pi u a^2 \quad (57)$$

$$\int \Omega ((x - R_0)^2 + y^2) d^2x = 4\pi u a \epsilon \left(\frac{a^2}{4} - \frac{2}{k^2} \right) . \quad (58)$$

Since the point vortex form is to approximate the FSW vortex, we can consider the initial state:

$$\Omega_p = \gamma_+ \delta (x - R_0 + b_+) \delta (y) + \gamma_- \delta (x - R_0 - b_-) \delta (y) \quad (59)$$

and enforce the equivalence of each of these three moments. For example, from the zeroth moment, we get $\int \Omega_p d^2x = 2\lambda$, and imposing equivalence to Eqn. (56), we obtain:

$$\lambda = \pi u a \epsilon . \quad (60)$$

Note that this can be solved for u , and since $u = \omega R_0$, we also have

$$\omega = \frac{\lambda}{\pi a^2} = \frac{\gamma_+ + \gamma_-}{2\pi a^2} \quad (61)$$

and comparing this to Eqn. (55), we get

$$d' = a , \quad (62)$$

which seems obvious, but is in fact nontrivial since $b_{\pm} \neq a/2$. In fact using the equivalence of the first moment as defined in Eqn. (57) and the fact that $b_- = a - b_+$, we obtain:

$$b_{\pm} = \frac{a}{2} \pm \frac{a}{\epsilon} \left[1 - \frac{\kappa}{2\pi u a} \right] . \quad (63)$$

Finally from the equivalence of the second moment as written in Eqn.(58), we get:

$$\gamma_+ b_+^2 + \gamma_- b_-^2 = 4\pi u a \epsilon \left(\frac{a^2}{4} - \frac{2}{k^2} \right) . \quad (64)$$

Substituting $\gamma_+ = \kappa + \lambda$, $\gamma_- = -\kappa + \lambda$, b_{\pm} from Eqn. (63) and λ from Eqn. (60), we can solve Eqn. (64) for κ as

$$\kappa = 2\pi u a \sqrt{\left(1 + \frac{4\epsilon^2}{k^2 a^2} \right)} . \quad (65)$$

When this is substituted back into (63) we obtain:

$$b_{\pm} = \frac{a}{2} \pm \frac{a}{\epsilon} \left[1 - \sqrt{\left(1 + \frac{4\epsilon^2}{k^2 a^2} \right)} \right] . \quad (66)$$

This means that the FSW vortex that is defined by u , a and ϵ as in Eqn. (35) can be represented by two point vortices as in Eqn. (59) where its parameters κ , λ and b_{\pm} are given by Eqns. (60), (65) and (66). It seems that this is slightly different from the

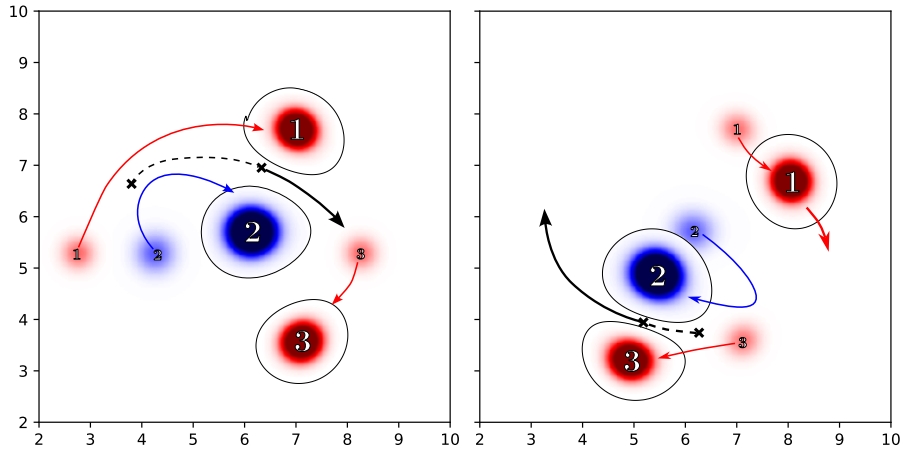


Figure 14. The vorticity evolution in a rotating tripolar cycle. The initial condition is shown on the left plot as a set of faint diffuse balls of vorticity labeled from 1 to 3. Initially 1 and 2 merge into a dipolar vortex moving in an elliptic orbit, while 3 drifts slowly downward. This state just before the collision is shown on the left in clear form with black contour lines. As the dipolar vortex catches up due to its intrinsic velocity, collision occurs, and 2 and 3 form a new dipole vortex leaving 1 behind. This final state is shown in clear form with black contour lines on the right plot (where the faint forms represent the previous state representing the final state of the left plot). The cycle then repeats with 3 playing the role of 1 and vice versa. A numerical implementation shows 10+ cycles without any deformation, apart from a slow upward drift. The movie version can be accessed in the online version of the paper (see Movie 8). Note that similar structures appear in simulations of sporadic turbulence shown in Movie 2 as well.

choice in Ref. 55 for the CL dipole. However since the CL dipole limit is degenerate (e.g. both the first and the second moments vanish), the choice, in that case, between the relative positions vs. the amplitudes is somewhat arbitrary and Ref. 55 decides to make sure the integrals over each half of the dipole are equivalent, which brings in the $H_1(j_{11}) \approx 1.09$ factor. In the case of the FSW vortex, one does not have a similar freedom and the point vortex given above seems to be the only choice.

6.4. A rotating tripole configuration

The first example of the collision between two rotating dipole vortices were initialized by four Gaussian stream function perturbations placed in a particular initial configuration so that they would form two dipole vortices moving in circular orbits that would eventually result in a collision. Similarly, we can start with three such perturbations instead of four in order to form tripolar vortices. It turns out that depending on the relative sizes and the initial distances of the three 'poles' involved in such an interaction, one gets different resulting configurations. For example if the system is initialized with a Gaussian stream function symmetrically in the middle of two Gaussian stream functions where the middle vortex is larger and has opposite vorticity to the two side vortices, the resulting configuration is a simple tripolar vortex⁵⁸. The whole configuration rotates in

the direction implied by its net vorticity. In contrast if one of the side vortices is moved further away, the system initially forms a dipole vortex type configuration between the two closer vortices, which moves in a circular trajectory and collides with the remaining one. During the collision the middle vortex exchanges its partner and continues in a circular orbit, encountering the original vortex that it left behind and again exchanging the new partner with the original one and so on. It keeps going in a circular orbit as shown in figure 14.

Note that such a configuration becomes obvious when we interpret it as an interaction among three point vortices, as it becomes a standard three body problem, which naturally has solutions of this form. In fact right after the initial evolution, which results in the expulsion of the outer rim of vorticity of each initial Gaussian stream function peak, we can replace the resulting vorticity maxima with point vortices and evolve the system as a three body problem. Many such solutions where the point vortices are organized in the form of crystals are also possible and well known in the study of superfluid helium and non-neutral plasmas.

7. Conclusion

The case of two dimensional turbulence that is extremely intermittent, either due to initial conditions, particularities of forcing or being in the process of transition results in a state that we call sporadic turbulence that is largely dominated by coherent structures, and in particular dipole vortices. It was shown that an initial state with localized patches of large amplitude turbulence rapidly evolves towards this state by formation of a number of these structures that are ejected from each patch through a mechanism of selective decay constrained by conservation of energy, enstrophy and circulation. We then observe that in this state of structure dominated two dimensional turbulence, most of the initial energy is localized in dipole vortices, that move around and interact mainly through collisions. The details of the formation process is discussed in section 4.1. It is shown that two Gaussian peaks of the stream function form dipole vortices if they are close enough. Analytical formulas for the parameters of the resulting dipole vortex such as the radius a , the propagation speed u and the radius of curvature R_0 , in terms of the parameters defining the initial condition such as the widths and amplitudes of the two Gaussian peaks are given for the inviscid limit in Eqns (28-30), and are shown to be consistent with the numerical observations with small viscosity whose effect is to slow down u and expand a . It was also shown that the effects of viscosity can be captured as a model friction on the dipole vortex resulting in a decay rate given in Eqn. (33).

Since the dipolar vortices have intrinsic momentum, they are ejected out of the region of initial concentration, or move in circular orbits until they encounter other dipolar or monopolar vortices or other features of large scale flow patterns. Interactions between dipole vortices usually results in other dipole vortices depending on the details of the collision as discussed in section 6.2, while the interaction between a dipole and a monopole may result in a tripole configuration as discussed in 6.4, the dipole exchanging

one of its poles with the monopole or the absorption of the monopole into the dipole. However depending on the details, one may also get narrow shear layers as by-products of these interactions.

Interactions between large scale sheared flows and dipole vortices are tricky. If the dipole is small enough, the result is the absorption of the dipole into the shear layer with slight modification on the large scale flow. But if the perturbation is large, the large scale flow structure may become unstable after the absorption of the dipole as shown in section 6.1. This provides a clear scenario for the transition from sporadic to standard Kraichnan-Kolmogorov type two dimensional turbulence with global dual cascade.

At the simplest level, a dipole vortex *can be approximated* as two monopolar point vortices that are apart by a distance d . In this sense the whole system can be considered as a gas of point vortices + a background flow pattern, whose evolution can be described by a Helmholtz formulation. However it is clear that the point vortex approximation is limited, and the back-reaction of a realistic dipole vortex on the rest of the flow, results in complex behavior that can not be described within such a framework.

We argue that a detailed understanding of dipole vortex is of key importance, because it appears as the only kind of coherent nonlinear structure that can perform self-propulsion. For example while an initial turbulent patch, would naturally spread in space through a phenomenon of nonlinear diffusion of eddies advecting one another coupled with inverse and forward cascades of different quantities, dipole vortices can propagate directly into regions of laminar flow while dragging along the seeds of turbulence either through their imperfections or by shedding of vorticity along their path. We also argue that their formation is not a curiosity that requires one to initialize the system in a very particular state in order to observe them. They are robust structures that naturally arise in the sporadic turbulence state. Therefore understanding of these structures, their interactions, and the interactions between them and more general flow structures should be an important aspect of the effort to understand two dimensional turbulence.

References

- [1] Frisch U 1995 *Turbulence: The Legacy of A. N. Kolmogorov* (Cambridge: Cambridge University Press)
- [2] She Z S and Leveque E 1994 *Phys. Rev. Lett.* **72** 336–339
- [3] Shen X and Warhaft Z 2002 *Physics of Fluids* **14** 370–381
- [4] Ishihara T, Gotoh T and Kaneda Y 2009 *Annual Review of Fluid Mechanics* **41** 165–180
- [5] Paret J and Tabeling P 1998 *Physics of Fluids* **10** 3126–3136
- [6] Boffetta G and Ecke R E 2012 *Annual Review of Fluid Mechanics* **44** 427–451 URL <https://doi.org/10.1146/annurev-fluid-120710-101240>
- [7] Diamond P H, S-I Itoh, Itoh K and Hahm T S 2005 *Plasma Physics and Controlled Fusion* **47** R35–R161

- [8] Gürçan Ö D and Diamond P H 2015 *Journal of Physics A: Mathematical and Theoretical* **48** 293001
- [9] Malkov M A, Diamond P H and Rosenbluth M N 2001 *Phys. Plasmas* **8** 5073–5076
- [10] Kobayashi S, Gürçan Ö D and Diamond P H 2015 *Physics of Plasmas* **22** 090702
- [11] Mandelbrot B B 1999 *Sporadic turbulence* (New York, NY: Springer New York) pp 290–291 ISBN 978-1-4612-2150-0
- [12] Carnevale G F, McWilliams J C, Pomeau Y, Weiss J B and Young W R 1991 *Phys. Rev. Lett.* **66** 2735–2737 URL <https://link.aps.org/doi/10.1103/PhysRevLett.66.2735>
- [13] Spineanu F and Vlad M 2017 *New Journal of Physics* **19** 025004 URL <https://dx.doi.org/10.1088/1367-2630/aa5a3d>
- [14] Taira K, Nair A G and Brunton S L 2016 *Journal of Fluid Mechanics* **795** R2
- [15] Kraichnan R H 1967 *Phys. Fluids* **10** 1417–1423
- [16] Kraichnan R H 1971 *Journal of Fluid Mechanics* **47** 525–535 ISSN 1469-7645
- [17] Bretherton F P and Haidvogel D B 1976 *Journal of Fluid Mechanics* **78** 129–154
- [18] Matthaeus W H and Montgomery D 1980 *Annals of the New York Academy of Sciences* **357** 203–222
- [19] Leith C E 1984 *The Physics of Fluids* **27** 1388–1395 URL <https://aip.scitation.org/doi/abs/10.1063/1.864781>
- [20] Carnevale G F, McWilliams J C, Pomeau Y, Weiss J B and Young W R 1992 *Physics of Fluids A : Fluid Dynamics* **4** 1314–1316 URL <https://doi.org/10.1063/1.858251>
- [21] Sipp D, Jacquin L and Cosssu C 2000 *Physics of Fluids* **12** 245–248 URL <https://doi.org/10.1063/1.870325>
- [22] Kraichnan R H and Panda R 1988 *The Physics of Fluids* **31** 2395–2397
- [23] Pelz R B, Yakhot V, Orszag S A, Shtilman L and Levich E 1985 *Phys. Rev. Lett.* **54** 2505–2508
- [24] Servidio S, Wan M, Matthaeus W H and Carbone V 2010 *Physics of Fluids* **22** 125107
- [25] Pushkarev A V and Bos W J T 2014 *Physics of Fluids* **26** 115102
- [26] Mason J, Cattaneo F and Boldyrev S 2006 *Phys. Rev. Lett.* **97** 255002
- [27] Leweke T, Le Dizès S and Williamson C H 2016 *Annual Review of Fluid Mechanics* **48** 507–541
- [28] Larichev V D and Reznik G M 1976 *Doklady Akademii Nauk SSSR* **231** 1077–1079
- [29] Sulem C and Sulem P L 1999 *The nonlinear Schrödinger equation* (Springer-Verlag)
- [30] Couder Y and Basdevant C 1986 *Journal of Fluid Mechanics* **173** 225–251
- [31] Ni Q, Zhai X, Wang G and Hughes C W 2020 *Journal of Geophysical Research: Oceans* **125** e2020JC016479

- [32] Kevrekidis P G, Carretero-González R, Frantzeskakis D J and Kevrekidis I G 2004 *Modern Physics Letters B* **18** 1481–1505
- [33] Neely T W, Samson E C, Bradley A S, Davis M J and Anderson B P 2010 *Phys. Rev. Lett.* **104** 160401
- [34] Meleshko V and van Heijst G 1994 *Journal of Fluid Mechanics* **272** 157–182
- [35] Flierl G R, Stern M E and Whitehead Jr J A 1983 *Dynamics of Atmospheres and Oceans* **7** 233–263 URL <http://www.sciencedirect.com/science/article/pii/0377026583900076>
- [36] Stuart J T 1967 *Journal of Fluid Mechanics* **29** 417–440
- [37] Onsager L 1949 *Il Nuovo Cimento* **6** 279–287
- [38] Zabusky N J and McWilliams J C 1982 *The Physics of Fluids* **25** 2175–2182 URL <https://aip.scitation.org/doi/abs/10.1063/1.863709>
- [39] Lydon K, Nazarenko S V and Laurie J 2022 *Journal of Physics A: Mathematical and Theoretical* **55** 385702 URL <https://dx.doi.org/10.1088/1751-8121/ac89bc>
- [40] Cerbus R T and Goldburg W I 2013 *Physics of Fluids* **25** 105111 URL <https://doi.org/10.1063/1.4824658>
- [41] Sofiadis G, Sarris I E and Alexakis A 2023 *Phys. Rev. Fluids* **8**(2) 024607
- [42] Juul Rasmussen J, Hesthaven J, Lynov J, Nielsen A and Schmidt M 1996 *Mathematics and Computers in Simulation* **40** 207–221 ISSN 0378-4754 URL <https://www.sciencedirect.com/science/article/pii/037847549500033X>
- [43] Hesthaven J S, Lynov J P, Nielsen A H, Rasmussen J J, Schmidt M R, Shapiro E G and Turitsyn S K 1995 *Physics of Fluids* **7** 2220–2229 URL <https://doi.org/10.1063/1.868470>
- [44] Hasegawa A and Wakatani M 1983 *Phys. Rev. Lett* **50** 682–686
- [45] Charney J G 1948 *Geofys. Publ. Oslo* **17** 1–17
- [46] Hasegawa A and Mima K 1978 *Phys. Fluids* **21** 87–92
- [47] Nielsen A H and Rasmussen J J 1997 *Physics of Fluids* **9** 982–991 URL <https://doi.org/10.1063/1.869193>
- [48] Nycander J and Isichenko M B 1990 *Physics of Fluids B: Plasma Physics* **2** 2042–2047 URL <https://doi.org/10.1063/1.859425>
- [49] Crowdy D G 1997 *International Journal of Engineering Science* **35** 141–149 ISSN 0020-7225
- [50] Haslam M C, Smith C J, Alobaidi G and Mallier R 2012 *International Journal of Differential Equations* **2012** 1 – 10 URL <https://doi.org/10.1155/2012/929626>
- [51] Abramowitz M and Stegun I A 1964 *Handbook of Mathematical Functions with Formulas, Graphs, and Mathematical Tables* ninth dover printing, tenth gpo printing ed (New York City: Dover)
- [52] Bajer K, Bassom A P and Gilbert A D 2004 *Journal of Fluid Mechanics* **509** 281–304

- [53] McWilliams J C and Zabusky N J 1982 *Geophysical & Astrophysical Fluid Dynamics* **19** 207–227 URL <https://doi.org/10.1080/03091928208208956>
- [54] Orlandi P and van Heijst G F 1992 *Fluid Dynamics Research* **9** 179 URL [https://dx.doi.org/10.1016/0169-5983\(92\)90004-G](https://dx.doi.org/10.1016/0169-5983(92)90004-G)
- [55] Meleshko V and van Heijst G 1994 *Chaos, Solitons & Fractals* **4** 977–1010 ISSN 0960-0779 special Issue: Chaos Applied to Fluid Mixing
- [56] Voropayev S I and Afanasyev Y D 1992 *Journal of Fluid Mechanics* **236** 665–689
- [57] Trieling R R, van Wesenbeeck J M A and van Heijst G J F 1998 *Physics of Fluids* **10** 144–159 URL <https://doi.org/10.1063/1.869556>
- [58] Kizner Z and Khvoles R 2004 *Phys. Rev. E* **70** 016307 URL <https://link.aps.org/doi/10.1103/PhysRevE.70.016307>